

REPORT DOCUMENTATION PAGE

Form Approved
OMB No. 0704-0188

Public reporting burden for this collection of information is estimated to average 1 hour per response, including the time for reviewing instructions, searching existing data sources, gathering and maintaining the data needed, and completing and reviewing this collection of information. Send comments regarding this burden estimate or any other aspect of this collection of information, including suggestions for reducing this burden to Department of Defense, Washington Headquarters Services, Directorate for Information Operations and Reports (0704-0188), 1215 Jefferson Davis Highway, Suite 1204, Arlington, VA 22202-4302. Respondents should be aware that notwithstanding any other provision of law, no person shall be subject to any penalty for failing to comply with a collection of information if it does not display a currently valid OMB control number. **PLEASE DO NOT RETURN YOUR FORM TO THE ABOVE ADDRESS.**

1. REPORT DATE (DD-MM-YYYY) 14-07-2005		2. REPORT TYPE Technical Report		3. DATES COVERED (From - To) Aug 03-Apr 05	
4. TITLE AND SUBTITLE Bonded Repair of Corrosion Grind-Outs				5a. CONTRACT NUMBER F05611-03-D-003	
				5b. GRANT NUMBER	
				5c. PROGRAM ELEMENT NUMBER	
6. AUTHOR(S) Mr. Stephan Verhoeven, M.S.				5d. PROJECT NUMBER	
				5e. TASK NUMBER	
				5f. WORK UNIT NUMBER	
7. PERFORMING ORGANIZATION NAME(S) AND ADDRESS(ES) Center for Aircraft Structural Life Extension (CASTLE) Department of Engineering Mechanics, HQ USAFA/DFEM 2354 Fairchild Drive, Suite 2J2, USAF Academy CO 80840-6240				8. PERFORMING ORGANIZATION REPORT NUMBER USAFA TR 2005-06	
9. SPONSORING / MONITORING AGENCY NAME(S) AND ADDRESS(ES) ASC/AAA 2145 Monahan Way Wright Patterson AFB, OH 45433-7017				10. SPONSOR/MONITOR'S ACRONYM(S)	
				11. SPONSOR/MONITOR'S REPORT NUMBER(S)	
12. DISTRIBUTION / AVAILABILITY STATEMENT Distribution A: APPROVED FOR PUBLIC RELEASE; DISTRIBUTION UNLIMITED					
13. SUPPLEMENTARY NOTES					
14. ABSTRACT The US Air Force is operating a large fleet of aging aircraft. Some examples of problems that aging aircraft can encounter are fatigue and corrosion. This research focuses on bonded repair of exfoliation corrosion in the upper wing skin of the E-8C Joint Star (B707) military transport aircraft. Upper wing skins on the E-8C have shown extensive exfoliation damage. According to Boeing, structural integrity could be compromised by further corrosion and fatigue cracking in case this damaged material is not removed. Therefore, the current approach to deal with this damage is to remove the exfoliated material by grinding it out, after which the removed material is not replaced. Depending on the location on the wing, local grind-outs are allowed, up to 25% of the skin thickness. However, if the exfoliation extends beyond this limit, this approach is no longer allowed since too much material is lost. An internal repair or wing plank replacement are the only repairs currently permitted by the Structural Repair Manual (SRM). Both repair options are very costly. The purpose of the current research is to develop a flush bonded repair method that restores structural integrity to corrosion grind-outs deeper than 25% of the skin thickness, so that severe corrosion cases can be handled without costly repair. A specimen was designed to simulate the predominantly compressive loading conditions in the upper wing skin. Grind-outs were made where 66% of the skin thickness was removed. Three types of repair were designed and bonded into the grind-outs: an aluminum repair, a boron-epoxy repair and a hybrid repair. The hybrid repair is a combination					
15. SUBJECT TERMS The i t t d d t t l i t d f t i l d i (b t t i d i) d Fatigue, corrosion, exfoliation, Structural Repair Manual (SRM), grind-out, hybrid repair, compression, boron-epoxy, constant amplitude fatigue loading					
16. SECURITY CLASSIFICATION OF:			17. LIMITATION OF ABSTRACT	18. NUMBER OF PAGES	19a. NAME OF RESPONSIBLE PERSON LtCol Scott A. Fawaz
a. REPORT Unclassified	b. ABSTRACT Unclassified	c. THIS PAGE Unclassified			19b. TELEPHONE NUMBER (include area code) 719.333.6266



DEPARTMENT OF THE AIR FORCE

THE DEPARTMENT OF ENGINEERING MECHANICS

USAF ACADEMY, COLORADO

17 AUG 2005

MEMORANDUM FOR DFEM COL FISHER

FROM: HQ USAFA/DFEM

SUBJECT: Public Release of Technical Report

Request permission to submit the attached technical report, "Bonded Repair of Corrosion Grind-Outs", to the Defense Technical Information Center (DTIC) for public release with unlimited distribution. The proposed report does not include any classified information, national security information, or policy statements.

Author: Verhoeven, Stephan

Title: Bonded Repair of Corrosion Grind-Outs

The report is to be published by the U.S. Air Force Academy in August 2005.

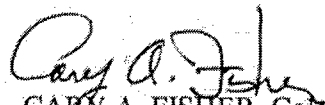


JASON B. AVRAM, Captain, USAF
Instructor of Engineering Mechanics

Attachment:
Technical Report

TO: DFEM (Capt Jason Avram)

Approved / ~~Disapproved~~



CARY A. FISHER, Colonel, USAF
Professor and Head

Distribution: Researcher, please maintain a copy of this completed letter for one year and forward a copy to the Director of Research for your department. Completion of an approval letter prior to public release is required by USAFA FOI 190-1.

Bonded Repair of Corrosion Grind-Outs

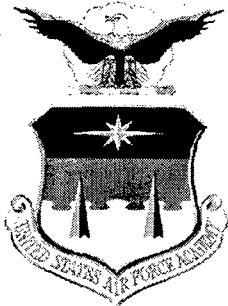
S. Verhoeven

Center for Aircraft Structural Life Extension (CAStLE)
Department of Engineering Mechanics

HQ USAFA/DFEM
2354 Fairchild Drive, Suite 6L-155
USAF Academy CO 80840-6240
(719) 333-6266, DSN 333-6266

April 2005

APPROVED FOR PUBLIC RELEASE; DISTRIBUTION UNLIMITED



DEAN OF THE FACULTY
UNITED STATES AIR FORCE ACADEMY
COLORADO 80840

20050825 044

Coordination and Approval

This article, *Bonded Repair of Corrosion Grind-Outs*, is presented as a competent treatment of the subject, worthy of publication. The United States Air Force Academy vouches for the quality of the research, without necessarily endorsing the opinions and conclusions of the authors. Therefore, the views expressed in this article are those of the authors and do not reflect the official policy or position of the United States Air Force, Department of Defense, or the US Government.

This report has been cleared for open publication and public release by the appropriate Office of Information in accordance with AFI 61-202 and USAFA FOI 190-1. This report may have unlimited distribution.

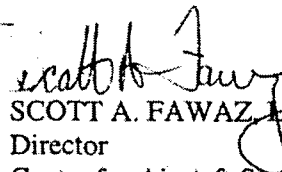
Prepared by:



S. Verhoeven
Senior Research Engineer

16 April 2005
Date

The report has been reviewed and is approved for publication.



SCOTT A. FAWAZ, Lt Col, USAF
Director
Center for Aircraft Structural Life Extension

16 April 2005
Date

Abstract

The US Air Force is operating a large fleet of aging aircraft. Some examples of problems that aging aircraft can encounter are fatigue and corrosion. This research focuses on bonded repair of exfoliation corrosion in the upper wing skin of the E-8C Joint Star (B707) military transport aircraft.

Upper wing skins on the E-8C have shown extensive exfoliation damage. According to Boeing, structural integrity could be compromised by further corrosion and fatigue cracking in case this damaged material is not removed. Therefore, the current approach to deal with this damage is to remove the exfoliated material by grinding it out, after which the removed material is not replaced. Depending on the location on the wing, local grind-outs are allowed, up to 25% of the skin thickness. However, if the exfoliation extends beyond this limit, this approach is no longer allowed since too much material is lost. An internal repair or wing plank replacement are the only repairs currently permitted by the Structural Repair Manual (SRM). Both repair options are very costly.

The purpose of the current research is to develop a flush bonded repair method that restores structural integrity to corrosion grind-outs deeper than 25% of the skin thickness, so that severe corrosion cases can be handled without costly repair.

A specimen was designed to simulate the predominantly compressive loading conditions in the upper wing skin. Grind-outs were made where 66% of the skin thickness was removed. Three types of repair were designed and bonded into the grind-outs: an aluminum repair, a boron-epoxy repair and a hybrid repair. The hybrid repair is a combination of aluminum and boron-epoxy. The specimens were tested under constant amplitude fatigue loading (both tension and compression) and under realistic spectrum fatigue loading, in order to come to the most efficient and durable repair concept.

It was found that a flush repair is a viable repair option for corrosion damage that is exceeding the current technical order (T.O.) limits, in a compression dominated structure. The fatigue tests showed that, from a durability standpoint, the best options are either a hybrid repair or an aluminum repair.

The test results show that boron-epoxy repairs should be avoided due to delamination problems under compressive fatigue loading. Furthermore, fatigue crack growth by compression-compression loading was observed. This is caused by the thermal residual stresses that are present after bonding.

Contents

Coordination and Approval.....	i
Abstract.....	ii
Contents	iii
List of Figures	v
List of Tables	vi
1. Introduction.....	1
2. Specimen Design	3
2.1 Corrosion Grind-Outs	3
2.2 Basic Specimen.....	5
2.3 Static Bending and Load Transfer Strain Measurements	9
2.4 Static Strain Measurements for Different Tapers	12
2.5 Design of Repairs.....	15
2.5.1 General Requirements and Guidelines.....	15
2.5.2 Materials Properties	16
2.5.3 Repair Design Process	17
2.6 Repairs	24
2.6.1 Aluminum Repair.....	24
2.6.2 Boron-Epoxy Repair	25
2.6.3 Hybrid Repair.....	26
2.7 Surface Preparation and Bonding	29
3. Fatigue Testing.....	32
3.1 Test Procedure	32
3.2 Test Matrix.....	34
4. Test Results and Discussion.....	36
4.1 CA Tension Tests.....	36
4.1.1 Specimens without Repairs.....	36
4.1.2 Specimens with Aluminum Repairs.....	36
4.1.3 Specimens with Boron-Epoxy Repairs	37
4.1.4 Specimens with Hybrid Repairs.....	38
4.2 CA Compression Tests	41
4.3 Spectrum Tests.....	43
5. Conclusions.....	47
6. Recommendations and Future Work	48
Acknowledgements.....	49
References.....	49
Appendix A: Crack Growth Data	50
A.1 Unpatched Specimens, CA Loading	50
A.2 Specimens with Aluminum Repairs, CA Loading.....	52
A.3 Specimens with Boron-Epoxy Repairs, CA Loading	54
A.4 Specimens with Hybrid Repairs, CA Loading.....	56
A.5 Unpatched Specimens, Spectrum Loading	58
A.6 Specimens with Aluminum Repairs, Spectrum Loading	59
A.7 Specimens with Boron-Epoxy Repairs, Spectrum Loading.....	60
A.8 Specimens with Hybrid Repairs, Spectrum Loading	61

Appendix B: C-Scan Images.....	62
B.1 Specimens with Aluminum Repairs, CA Tension Loading	62
B.2 Specimens with Aluminum Repairs, CA Compression Loading.....	63
B.3 Specimens with Aluminum Repairs, Spectrum Loading	64
B.4 Specimens with Boron-Epoxy Repairs, CA Tension Loading.....	66
B.5 Specimens with Boron-Epoxy Repairs, CA Compression Loading	67
B.6 Specimens with Boron-Epoxy Repairs, Spectrum Loading	68
B.7 Specimens with Hybrid Repairs, CA Tension Loading	69
B.8 Specimens with Hybrid Repairs, CA Compression Loading	70
B.9 Specimens with Hybrid Repairs, Spectrum Loading	71

List of Figures

Figure 1: The E-8C Joint Star reconnaissance aircraft	1
Figure 2: Example of exfoliation corrosion on upper wing skin	2
Figure 3: Wing panel locations for B707.....	3
Figure 4: Grind-out for aluminum repair	
Figure 5: Grind-out for boron and hybrid repair.....	5
Figure 6: Specimen dimensions.....	7
Figure 7: Anti-buckling test set-up	8
Figure 8: Strain gage locations	9
Figure 9: Strain gage locations (note that the tests were performed without the rivet holes present)	12
Figure 10: Membrane and bending strains for location 1 for panels with double and single taper.....	13
Figure 11: Membrane and bending strains for location 0 for panels with double and single taper.....	14
Figure 12: Membrane and bending strains for location 4 for panels with double and single taper.....	14
Figure 13: Relationship between transfer length, overlap length and patch length [C5033] .	20
Figure 14: Aluminum repair before and after bonding.....	24
Figure 15: Boron-epoxy repair after bonding.....	25
Figure 16: Hybrid patch concept for a compression dominated structure	26
Figure 17: Boron-epoxy plies of the patch with one layer of EA9696 adhesive. Note the hi-loks at the bottom of the grind-out.....	28
Figure 18: Boron-epoxy plies at bottom of grind-out, aluminum ply with EA9696 adhesive ready to be fitted. Note that the aluminum layer is longer than the boron-epoxy.	28
Figure 19: Hybrid patch installed	29
Figure 20: Heatcon vacuum table	30
Figure 21: Specimen with aluminum repairs in vacuum table	31
Figure 22: Specimen with bonded repair in c-scan tank.....	33
Figure 23: MTS 810 110 kip hydraulic load frame	33
Figure 24: Specimens without repair, CA loading.....	39
Figure 25: Specimens with aluminum repairs, CA loading.....	39
Figure 26: Specimens with boron-epoxy repairs, CA loading.....	40
Figure 27: Specimens with hybrid repairs, CA loading.....	40
Figure 28: Crack growth curves for specimens with and without repairs, CA loading.....	41
Figure 29: C-Scan of boron-epoxy repair before and after compression test.....	42
Figure 30: Boron-epoxy patch after compression test	42
Figure 31: Specimens without repair, spectrum loading	44
Figure 32: Specimens with aluminum repairs, spectrum loading.....	44
Figure 33: Specimens with boron-epoxy repairs, spectrum loading.....	45
Figure 34: Specimens with hybrid repairs, spectrum loading.....	45
Figure 35: Spectrum specimens with three different repairs, spectrum loading.....	46
Figure 36: Spectrum specimens with and without repairs, spectrum loading	46

List of Tables

Table 1: Percentage bending as function of applied tensile stress.....	10
Table 2: Percentages of load transfer as function of applied tensile stress.....	10
Table 3: Percentage bending as function of applied compressive stress	11
Table 4: Percentage load transfer as function of applied compressive stress	11
Table 5: Material properties for specimen and patch materials.....	16
Table 6: Properties for adhesive Hysol EA 9696 0.06 psf (R.T. properties).....	16
Table 7: Constant Amplitude Test Specimens.....	35
Table 8: Spectrum Test Specimens.....	35
Table 9: a-N data for specimen CA1	50
Table 10: a-N data for specimen CA2	50
Table 11: a-N data for specimen CA3	50
Table 12: a-N data for specimen CA4	51
Table 13: a-N data for specimen CA5	52
Table 14: a-N data for specimen CA6	52
Table 15: a-N data for specimen CA7	52
Table 16: a-N data for specimen CA8	53
Table 17: a-N data for specimen CA9	54
Table 18: a-N data for specimen CA10	54
Table 19: a-N data for specimen CA11	55
Table 20: a-N data for specimen CA12	55
Table 21: a-N data for specimen CA13	56
Table 22: a-N data for specimen CA14	56
Table 23: a-N data for specimen CA15	57
Table 24: a-N data for specimen CA16	57
Table 25: a-N data for specimen S1.....	58
Table 26: a-N data for specimen S2.....	58
Table 27: a-N data for specimen S3.....	59
Table 28: a-N data for specimen S4.....	59
Table 29: a-N data for specimen S5.....	59
Table 30: a-N data for specimen S6.....	60
Table 31: a-N data for specimen S7.....	60
Table 32: a-N data for specimen S8.....	61
Table 33: a-N data for specimen S9.....	61
Table 34: a-N data for specimen S10.....	61

1. Introduction

The US Air Force is operating a large fleet of aging aircraft. Some examples of problems that aging aircraft can encounter, among others, are fatigue and corrosion. This research focuses on bonded repair of exfoliation corrosion in the upper wing skin of the E-8C Joint Star (B707) military transport aircraft (Figure 1). In the past, bonded repairs have shown to be a very effective repair method, in situations where riveted repairs did not work, and/or replacement of the part was cost prohibitive or impossible due to the lack of replacement parts.

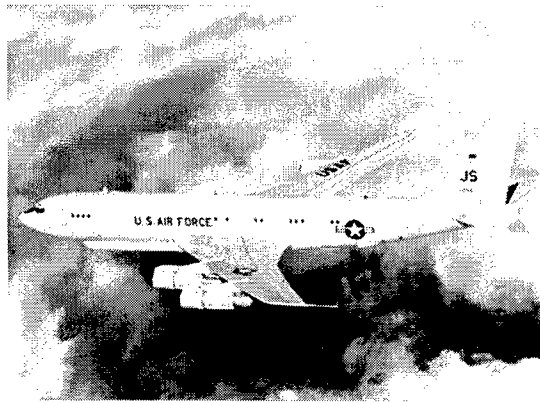


Figure 1: The E-8C Joint Star reconnaissance aircraft

Upper wing skins on the E-8C, made out of 7075-T6 (and 7178-T6 on earlier aircraft) aluminum, have shown extensive exfoliation damage, mainly around the fastener holes, see Figure 2. Exfoliation corrosion is a form of intergranular corrosion associated with high strength aluminum alloys. Heavily worked alloys with a microstructure of elongated grains are especially susceptible to exfoliation. Corrosion products will build up along the grain boundaries and eventually result in layers of the material peeling or flaking off. Exfoliation often initiates at end grains encountered in locations such as machined holes, and can progress further into the material.

According to a Boeing Service Letter [1], structural integrity could be compromised by corrosion and fatigue cracking from unrepaired damage. Therefore, the current approach to deal with this damage is to remove the exfoliated material by grinding it out, after which the removed material is not replaced. Depending on the location on the wing, local grind-outs are allowed--up to 25% of the skin thickness (see also reference [2] for more details on specific locations and grind-out limits).

However, if the exfoliation extends beyond this limit, this approach is no longer allowed since too much material is lost. Replacement of the wing plank might be necessary, making this damage very costly.

The purpose of the current research is to develop a flush bonded repair method that restores structural integrity to corrosion grind-outs deeper than 25% of the skin thickness, so that severe corrosion cases can be handled without the possible need for wing plank replacement or costly repair.

Repairs were designed using accepted design procedures (discussed in the Composite Repair to Metallic Structures handbook CRMS [3] and the Royal Australian Air Force (RAAF) C5033 Engineering Standard [4]), and specimens were tested in fatigue in order to come to the most efficient and durable repair concept.

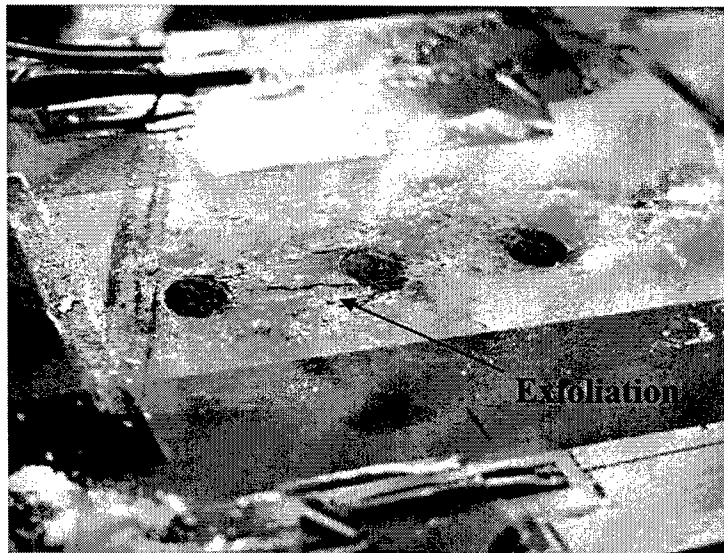


Figure 2: Example of exfoliation corrosion on upper wing skin

2. Specimen Design

2.1 Corrosion Grind-Outs

In order to come to the most efficient and durable repair concept for corrosion grind-outs, the efficiency and fatigue durability of the different repairs were determined by testing.

Since the dimensions of the specimen are driven by the size of the damage, in this case the corrosion grind-out, it was necessary to look at field data in order to determine the dimensions of a representative grind-out.

The area of interest for this project was wing station (WS) 320, wing panel 11JBD and wing panel 11JBF (see Figure 3 and [2] for the panel locations). Note however that the repair concepts that will be developed here will be more widely applicable, to include other areas of the upper wing skin.

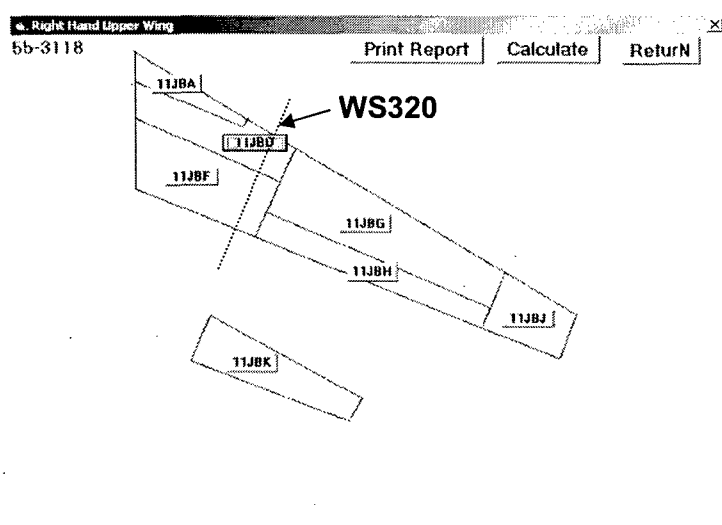


Figure 3: Wing panel locations for B707

In-service grind-out data from the Tinker AFB Grind-Out Data Base was supplied by S&K Technologies. Analysis of the grind-out dimensions of in-service aircraft showed that for panel 11JBD, 31 out of 669 grind-outs were larger than 50.8 mm (2") in diameter, therefore 95.4% of the grind-outs were smaller than 50.8 mm in diameter. Also, the deepest grind-out found on panel 11JBD was 1.27 mm (0.05") deep.

For panel 11JBF, 97 out of 1104 grind-outs were larger than 50.8 mm in diameter, and thus 91.2% of the grind-outs on this panel were smaller than 50.8 mm in diameter. The deepest grind-out found on panel 11JBF was 3.23 mm (0.127") deep.

Current T.O. guidelines [2] prescribe the following requirements for corrosion grind-outs:

- Remove all corrosion
- Add blend-out length of 10 times the grind-out depth in loading direction
- Add blend-out length of 5 times the grind-out depth perpendicular
- Grind-out is elliptical in shape
- Grind-out needs to be terminated between rivets
- Re-countersink fastener if countersink ≤ 0.75 times the remaining thickness

In order to significantly expand the current T.O. limits for corrosion grind-outs, the grind-out depth was increased from 25% to 66% of the skin thickness. The specimen (wing skin) material for this project was 7075-T6 bare, with a 4.826 mm (0.19") thickness, therefore resulting in a 3.175 mm (0.125") deep grind-out.

To shape the grind-outs for this project, it was assumed that two adjacent fastener holes have corrosion damage with a diameter of 50.8 mm, see the overlapping circles in Figure 4 and Figure 5. The area covered by these 2 circles was then approached by a rectangular area in which the corrosion depth was assumed constant with a depth of 3.175 mm. The blend out lengths were then added. The use of a rectangular patch is preferred because the edges of circular patches are inefficient, due to the absence of sufficient overlap length along the edges.

Following the T.O. requirements of tapering in two directions resulted in a grind-out that is shaped as a pyramid-without-top (Figure 4). By omitting the taper perpendicular to loading direction, the second type of grind-out was formed (Figure 5).

Both grind-outs had a taper of 10:1 in loading direction. Leaving out the taper in width direction (5:1 taper ratio) makes it easier to fit the composite and hybrid patches (see paragraph 2.6). Static strain gage measurements in and around these two grind-outs showed differences smaller than 5% for the two most important locations (the center of the grind-out and at the run-out of the grind-out). More details can be found in [5] and paragraph 2.4.

The remaining thickness in the bottom of the grind-out is sufficient to allow re-countersinking of the hi-loks without creating a knife-edge condition. The height of the head of HL19PB-6-6 Hi-Loks is 0.047", the remaining skin thickness is $0.19" - 0.125" = 0.065"$ and thus 75% of the remaining thickness is $0.04875"$, satisfying the T.O. requirements.

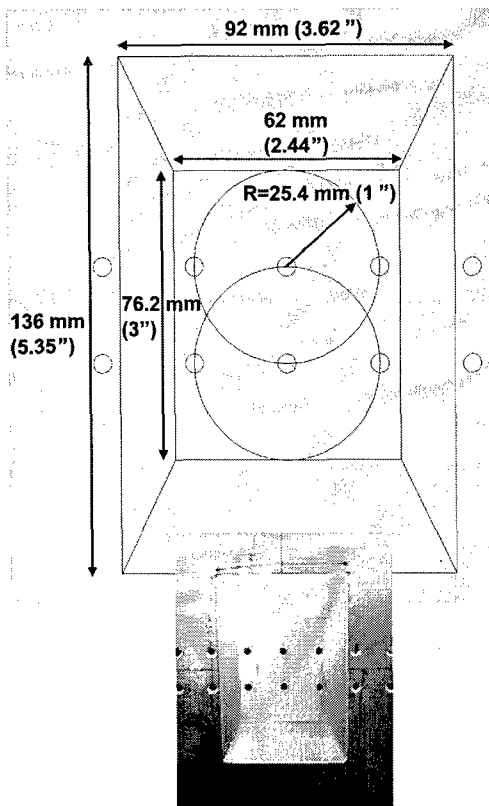


Figure 4: Grind-out for aluminum repair

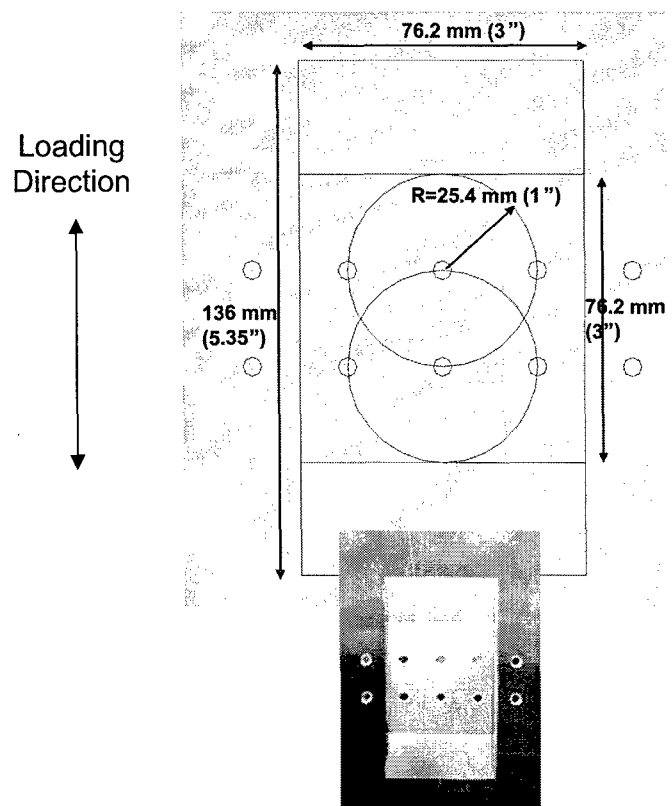


Figure 5: Grind-out for boron and hybrid repair

2.2 Basic Specimen

Now that the damage size, in this case the size of the corrosion grind-outs, has been determined, the actual test specimen can be sized. The specimen had to be designed to simulate the loading conditions in the upper wing skin. Since the upper wing skin is predominantly loaded in compression, the specimen had to be able to withstand significant compressive loads. Furthermore, since the exfoliation occurs mainly around fastener holes, a mechanically fastened joint had to be designed and the repairs had to be flush with or within the contour of the wing skin.

Because the specimens were not designed to be an exact replica of the actual structure in the upper wing skin, but to replicate the loading conditions in the wing skin, it was decided to use an unstiffened panel. When testing a significant number of specimens, it is important that the specimens are relatively easy to manufacture and inspect. When applying a bonded repair using a vacuum table (to simulate the bonding conditions on an actual aircraft as close as possible), not having a stiffener on the back of the wing skin will make the application of pressure on the repaired area much easier. Also, inspecting damage under the repair using eddy current NDI (non-destructive inspection) will be easier without the stiffener present.

The specimen had to meet the following requirements:

- Mechanically fastened joint
- Less than 10% load transfer over each rivet row
- Less than 10% secondary bending
- Maximum compressive stress of -193 MPa (-28 ksi) (minimum spectrum stress)
- Maximum tensile stress of 115.8 MPa (16.8 ksi) (maximum spectrum stress)
- The repair that is applied must be flush with the contour of the wing skin

Aluminum 7075-T6 bare, with a thickness of 4.826 mm (0.19") was used as specimen/skin material. The fasteners that are used on the actual aircraft are lock bolts. The front and rear spar chords are typically 3/16" diameter lock bolts, stringer 12 uses 1/4" diameter lock bolts, and the WS 360 break uses lock bolts in the range from 3/16" up to 5/16" diameter.

For this project an equivalent Hi-Lok fastener, HL19PB-6-6, with a diameter of 3/16" was used, combined with a HL70-6 collar. Spacer rings were used to bring the total thickness of the specimen within the required grip length.

The specimen had to be wide enough to allow for load attraction (in case of a stiff inclusion, e.g. repaired area) or load bypass (in case of a compliant/flexible inclusion, e.g. grind-out). Also, the specimen had to be sufficiently long to have a uniform stress distribution across the width of the specimen, away from the grips.

Figure 6 shows the dimensions of the specimen with a single bolt row in the grip area. These specimens were used for tests where there was no load reversal, only tension-tension or compression-compression. There were also specimens with a double row of bolts to prevent the specimen from slipping in the grips when the loads are changing direction. The extra two rows were added to each end of the specimen, making the total length of the specimen 660.4 mm (26"). Note that the gage length of the specimens (length of free specimen between the steel grips) remained the same for both configurations, 501.5 mm (19.75")

In order to create the necessary load transfer through the hi-loks, a sheet of 2024-T3 bare aluminum with a thickness of 1 mm (0.04") was attached to the specimen. The length of this thin sheet is half the specimen length plus 25.4 mm (1"), see Figure 6. The thin sheet was fastened using two rows of nine hi-loks, centered around the horizontal centerline of the specimen. The rivet pitch was 25.4 mm (1").

Since the specimen would not be able to withstand the high compressive loads, anti-buckling plates combined with four I-beams were used to support the specimen, see Figure 7. The two steel anti-buckling plates, each with a thickness of 12.7 mm (0.5"), were attached to either side of the specimen. The steel plates were covered with Teflon sheets to prevent friction build-up. The plates were attached using two rows of bolts that are hand-tightened. To avoid friction between the anti-buckling plates and specimen, it is important not to clamp the anti-buckling plates onto the specimen. Clamping the anti-buckling plates onto the specimen could lead to load transfer through the steel plates, which is unwanted. The limited amount of play that is necessary between the plates and specimen will result in the desired amount of bending in the specimen.

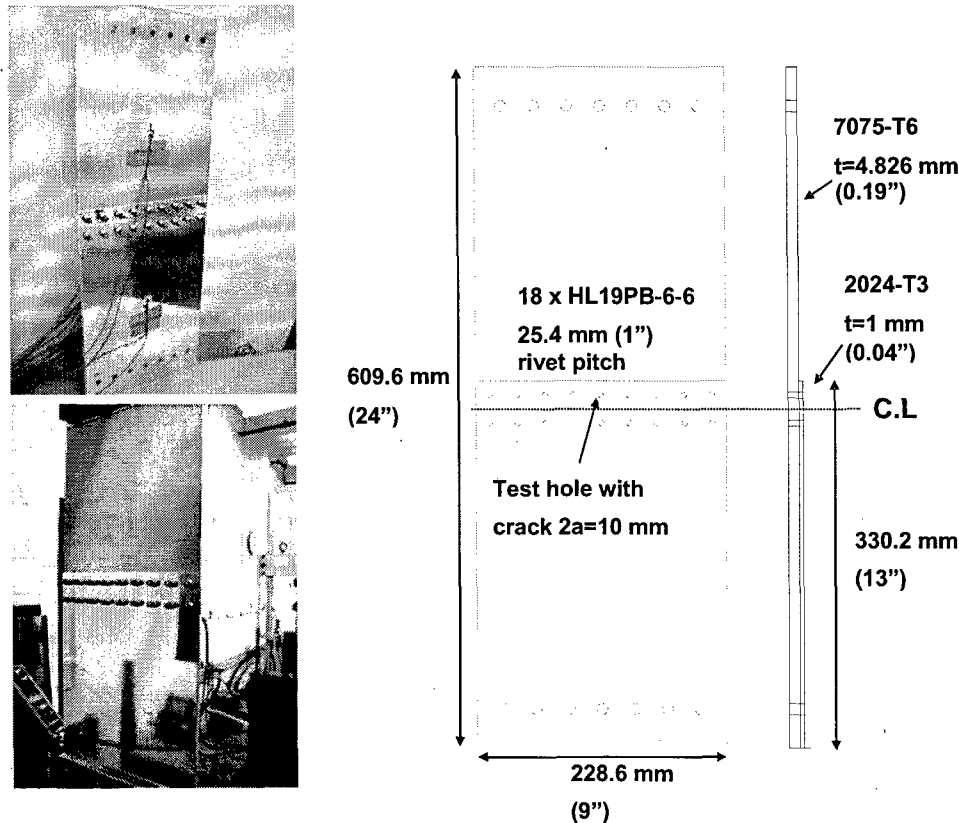


Figure 6: Specimen dimensions

To prevent loading the plates in compression, the anti-buckling plates were shorter than the specimen gage length. The small gap that allowed for this, was cause for some bending near the grips. For that reason four I-beams were bolted onto the grips, fixed to the grips on one side, and sliding in slots on the other side of the specimen. Strain gage measurements were taken along the length of the specimen to verify that the loading requirements were met.

As can be seen in Figure 6, the top center rivet hole had a through-crack on both sides of the hole. There were several reasons for making a starter crack in this location:

- To compare the effectiveness of the different types of repairs, crack growth rates were compared.
- If no crack would be present, one would be looking at a crack nucleation event, which can have large amounts of scatter.
- Having a starter crack represents a worst case scenario: a crack has initiated in the substrate. Can the repair control this crack over the remaining life time?

The total length $2a$ of the crack, including the rivet hole, is 10 mm (0.4"). All the starter cracks were pre-cracked at 80 MPa (11.6 ksi), $R=0.05$, to avoid large plastic zones. The grind-outs were made after pre-cracking.

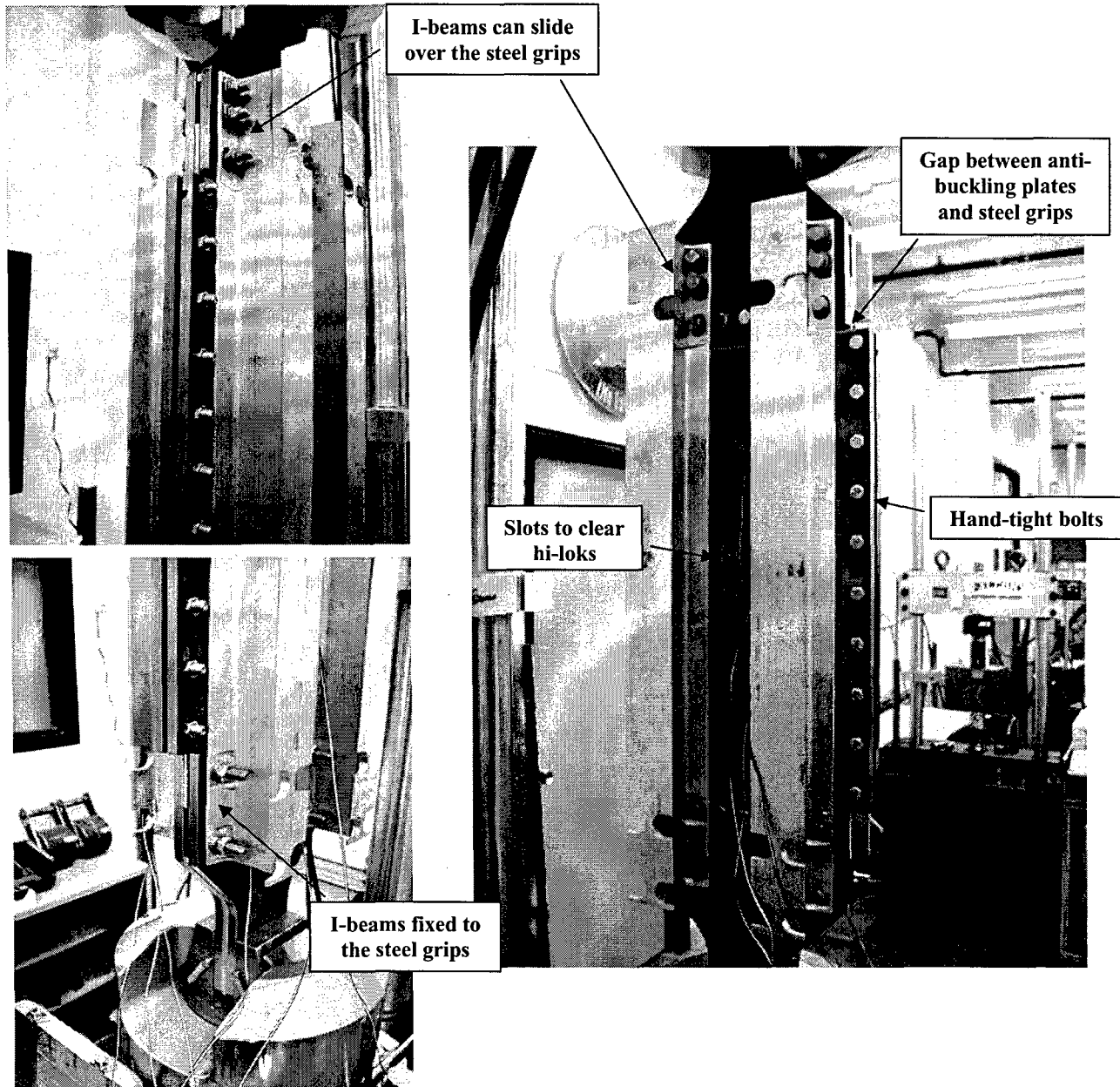


Figure 7: Anti-buckling test set-up

2.3 Static Bending and Load Transfer Strain Measurements

To verify that the loading requirements were met, a specimen was instrumented with 6 strain gages (Micro-Measurements CEA-13-125UN-350). The gages were placed along the length of the specimen, location 1 and 3 are located on the vertical center line of the specimen, location 2 is on the horizontal center line of the specimen but is offset 12.7 mm (0.5") in horizontal direction (half the rivet pitch).

Gages are mounted back to back so that bending strains can be measured. Also note that locations 2 and 3 are in the area where the 1.0 mm (0.04") thin sheet is mounted. Holes were made in the thin sheet to allow the strain gage wires to be routed.

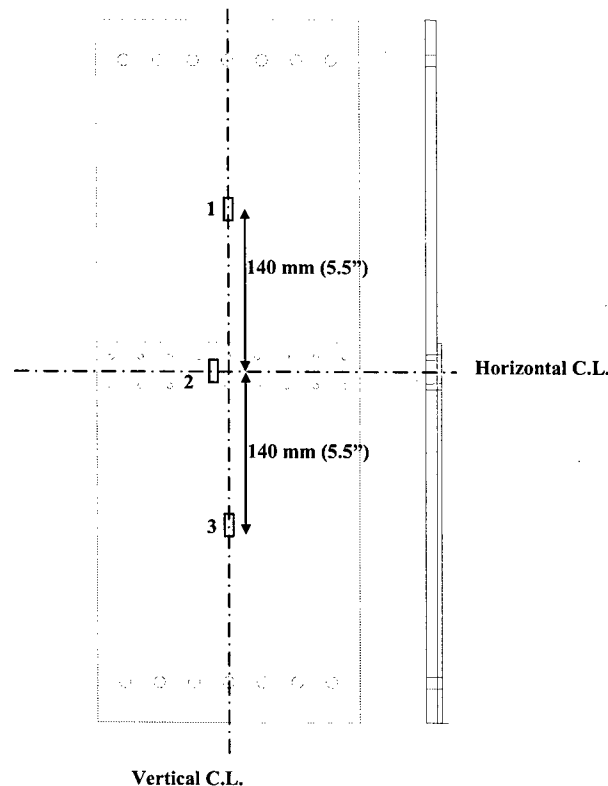


Figure 8: Strain gage locations

Table 1 and Table 2 show the results for tensile loading of the specimen. As can be seen, bending is slightly higher than desired at the lower stress levels but falls within the requirement at the higher stress levels. What can also be seen is that the bending varies somewhat along the length of the specimen, which is due to the fact that the I-beams are bolted down on the grips at one end of the specimen (closest to location 3), and sliding, and therefore not bolted down at the other end of the specimen (closest to location 1). Remember

that the steel anti-buckling plates are not clamped down on the specimen, which allows for limited out-of-plane movement and therefore bending.

As can be seen from Table 2, the percentage of load transfer for both rivet rows is close to or within the requirements for all load levels. The second column shows the total amount of load transfer for the joint (the two rivet rows combined), calculated by comparing location 3 to location 1. The third and fourth column shows the percentage of load transfer for the individual rivet rows. As can be seen, the top rivet row is transferring less load than the bottom rivet row. Column five and six show the contribution of the individual rows in the total load transfer of the joint. The top rivet row is transferring slightly over a third of the total load that is being transferred through this rivet joint.

Table 1: Percentage bending as function of applied tensile stress

Tensile Test Applied Stress (MPa)	Location 1 Percentage Bending	Location 2 Percentage Bending	Location 3 Percentage Bending
0	0	0	0
20	8.68	15.93	0.83
40	5.28	13.81	0.63
60	3.16	11.98	0.83
80	1.80	10.40	0.98
100	0.92	9.25	1.01
120	0.28	7.85	0.90

Table 2: Percentages of load transfer as function of applied tensile stress

Tensile Test Applied Stress (MPa)	Total percentage of load transfer for two rivet rows combined (position 3 compared to 1)	Percentage of load transfer for top rivet row (position 2 compared to position 1)	Percentage of load transfer for bottom rivet row (total load transfer minus load transfer percentage for top row)	Contribution (%) of top rivet row in total load transfer	Contribution (%) of bottom rivet row in total load transfer
0	0	0	0	0	0
20	16.67	6.25	10.42	37.50	62.50
40	16.88	5.97	10.91	35.38	64.62
60	16.83	6.03	10.80	35.84	64.16
80	16.74	6.16	10.58	36.83	63.17
100	16.00	6.13	9.87	38.30	61.70
120	15.73	5.82	9.91	36.98	63.02

Table 3 and Table 4 show the results for compressive loading of the specimen. As can be seen again, bending in the test area is slightly higher than desired at the lower stress levels but falls within the requirement at the higher stress levels. What can be seen here as well is that the bending varies along the length of the specimen.

As can be seen from Table 4, the percentage of load transfer is very close to or within the requirements for all load levels. Again, the top rivet row is transferring less load than the bottom rivet row but the difference between the two rows is smaller than for the tension situation, especially at the higher applied stress levels, where the contribution of each row is close to half of the total load transfer for the joint.

Table 3: Percentage bending as function of applied compressive stress

Compressive Test Applied Stress (MPa)	Location 1 Percentage Bending	Location 2 Percentage Bending	Location 3 Percentage Bending
0	0	0	0
-20	12.24	17.01	1.26
-40	13.74	16.09	1.04
-60	9.31	13.72	1.52
-80	4.96	10.95	1.70
-100	3.41	8.59	3.65
-120	1.79	7.65	2.41
-140	0.17	7.11	1.48
-160	2.52	6.49	1.11
-180	4.73	6.00	5.77
-200	6.31	5.49	8.89

Table 4: Percentage load transfer as function of applied compressive stress

Compressive Test Applied Stress (MPa)	Total percentage of load transfer for two rivet rows combined	Percentage of load transfer for top rivet row (position 2 compared to position 1)	Percentage of load transfer for bottom rivet row (total load transfer minus load transfer percentage for top row)	Contribution (%) of top rivet row in total load transfer	Contribution (%) of bottom rivet row in total load transfer
0	0	0	0	0	0
-20	16.78	6.47	10.31	38.54	61.46
-40	16.01	5.95	10.06	37.16	62.84
-60	15.83	6.23	9.60	39.34	60.66
-80	15.62	6.57	9.05	42.06	57.94
-100	15.18	6.95	8.23	45.77	54.23
-120	14.78	7.00	7.78	47.36	52.64
-140	14.44	6.80	7.64	47.08	52.92
-160	14.29	6.67	7.62	46.66	53.34
-180	14.24	6.59	7.65	46.27	53.73
-200	14.34	6.62	7.72	46.17	53.83

2.4 Static Strain Measurements for Different Tapers

As was mentioned already in paragraph 2.1, two different tapers were used for the grind-outs, see Figure 4 and Figure 5. To verify that the strains in and around these two different types of grind-outs were not significantly different; specimens were tested with back-to-back mounted strain gages in order to determine the membrane and bending strains. Specimens were loaded up to a stress level of 120 MPa (17.4 ksi).

Figure 9 shows the three strain gage locations that are most interesting: location 1 at the center of the grind-out; location 0 on the vertical centerline of the grind-out at the tip of the grind-out; location 4 at the corner of the grind-out. More specific information about the locations of these and additional gages can be found in [5].

For the grind-out with double taper, location 4 was located at the corner of the two intersecting tapers. Also note that the strains were measured without the rivet holes present.

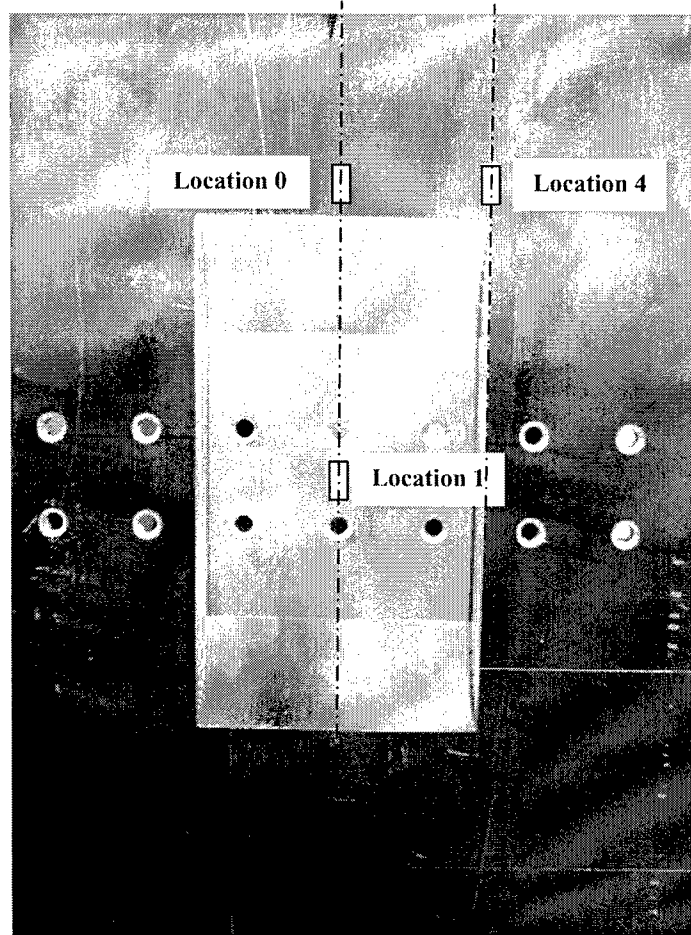


Figure 9: Strain gage locations (note that the tests were performed without the rivet holes present)

Figure 10 shows the strain-load data for location 1 for the two different grind-outs. At the maximum applied load, the grind-out with single taper has a membrane strain that is approximately 4.8% lower than the membrane strain for the grind-out with double taper. Apparently, the grind-out with double taper, which is a little bit wider than the grind-out with single taper, allows for a slightly lower amount of load bypass. It can also be seen that the bending in the center of the grind-outs is almost zero but it must be noted that there is no thin half sheet attached.

Figure 11 shows the membrane and bending strains at the run-out of the grind-out. It can be seen that the difference in membrane stresses is less than 1% at the maximum applied load. There is, as expected, a significant amount of secondary bending but the amounts of bending are very close to each other for the two different types of grind-outs.

Figure 12 shows the membrane and bending strains, measured in loading direction, at location 4, the corner of the grind-out. It can be seen that the membrane strains are approximately 8% lower for the grind-out with the single taper compared to the double taper grind-out. Bending strains are almost identical at the highest applied load.

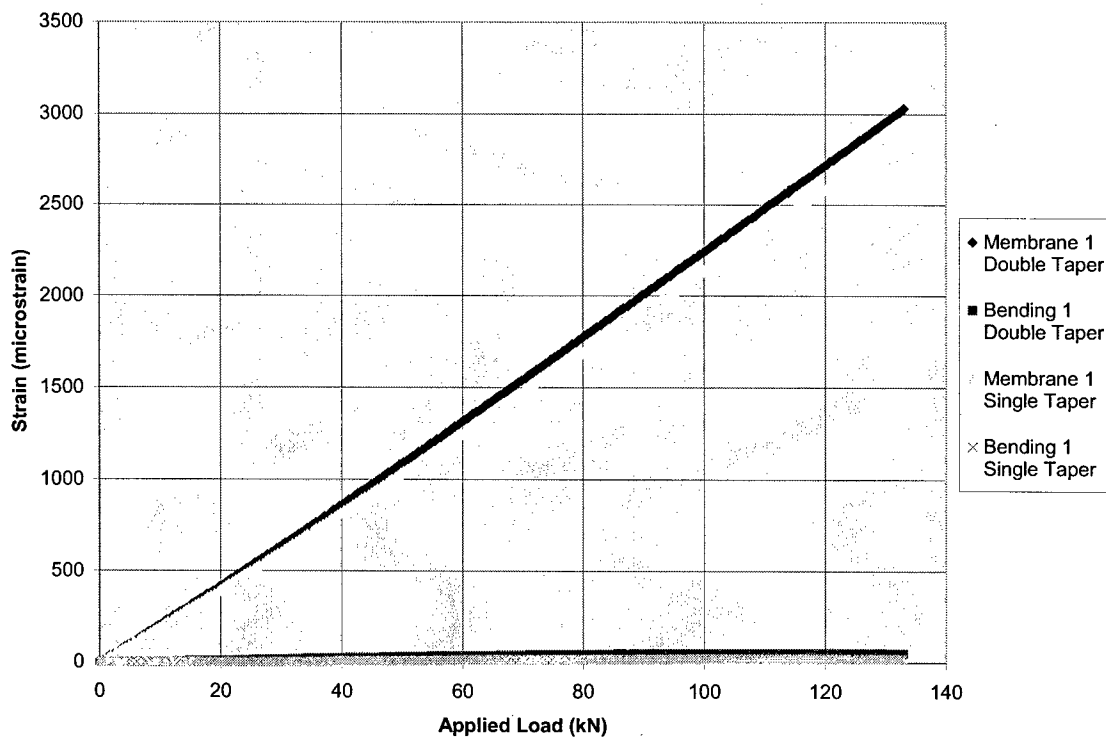


Figure 10: Membrane and bending strains for location 1 for panels with double and single taper

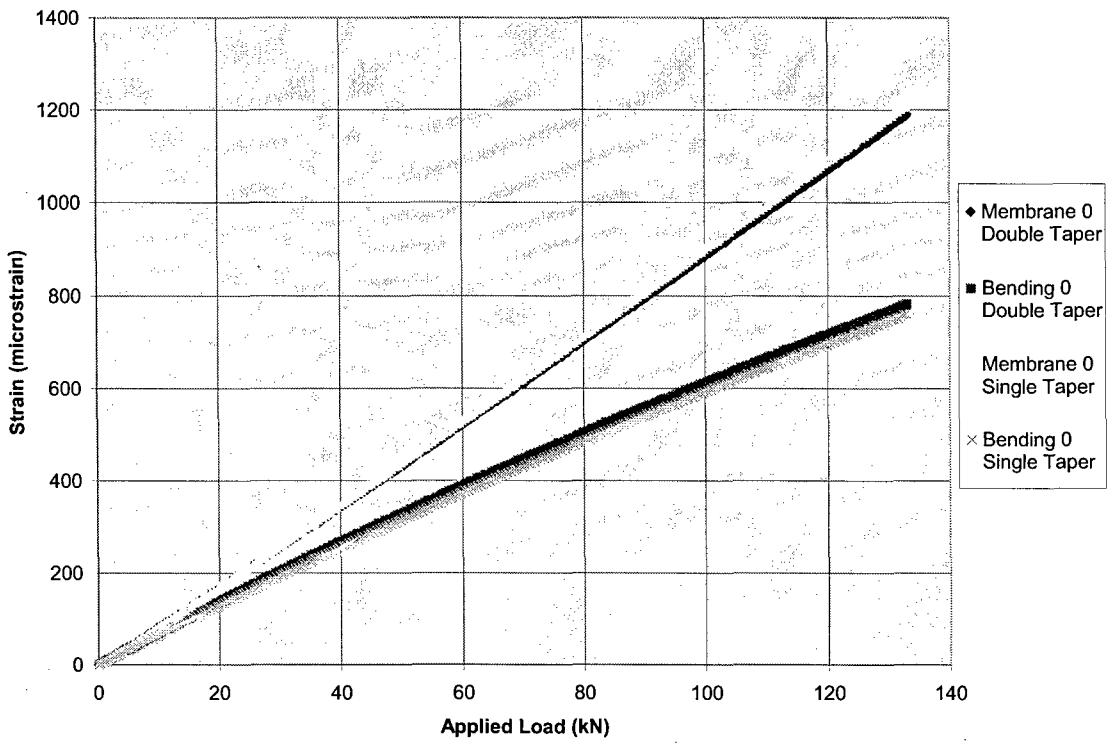


Figure 11: Membrane and bending strains for location 0 for panels with double and single taper

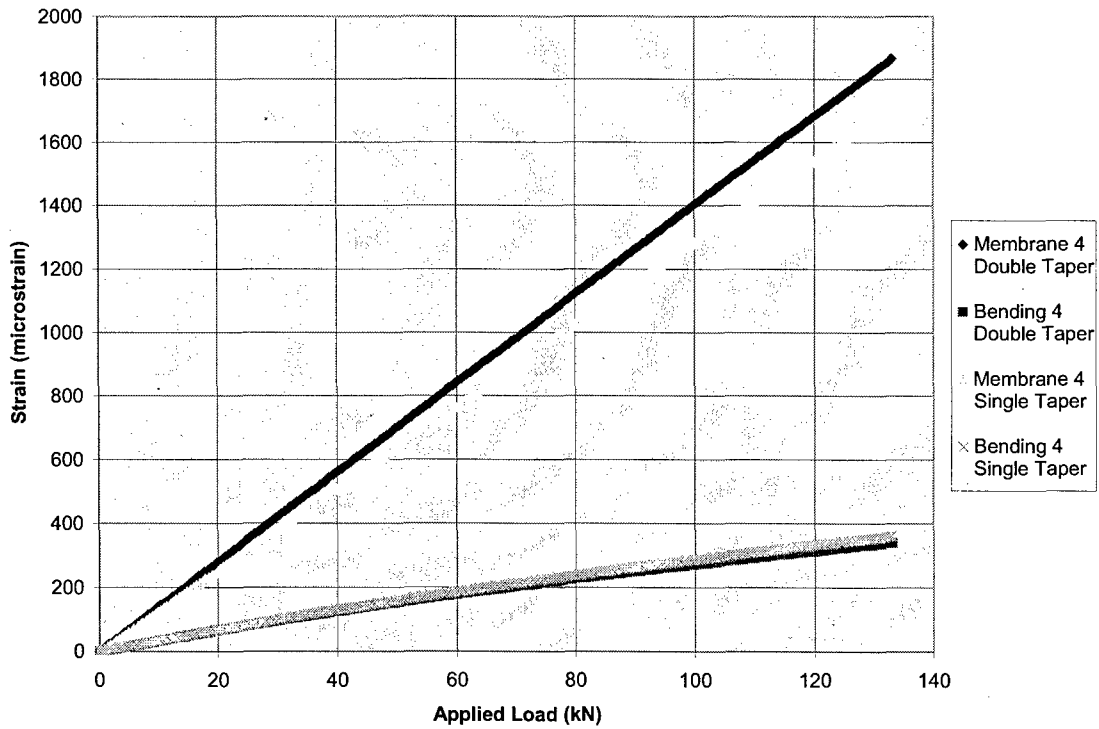


Figure 12: Membrane and bending strains for location 4 for panels with double and single taper

2.5 Design of Repairs

2.5.1 General Requirements and Guidelines

In order to design the repairs for the grind-outs, several requirements had to be met:

- Repairs must be flush with the contour of the wing. The structural repair manual (SRM) does allow for temporary external patches on the wing surface, up to 0.125 inches thick but recommends that the temporary patch is replaced with a flush mounted repair at the next major maintenance cycle. The flushness requirement does limit the possibilities for repairs.
- Repair must fit within the grind-out:
 - It was decided to follow the current T.O. guidelines for taper angles when making the grind-outs.
 - Only the “corroded” material is removed so that the grind-out is kept as small as possible. The grind-out is not made any larger to facilitate the bonded repair, which is not ideal. Therefore the repairs shown in this paper are designed to sustain the loading and temperature conditions mentioned before, repairs could need re-sizing depending on specific location/loading/operating conditions on the aircraft.
- Repair is sized to carry loads that are normally carried by the removed material, assuming that the remaining material is undamaged.
- In order to size the repairs, a combination of the CRMS handbook [3] and the RAAF Engineering Standard C5033 [4] was used. All equations used in this report can be found in these two manuals.

Since the assumption is that the grind-out is not made any larger than strictly necessary to remove the corroded area and add the taper, the in-plane dimensions of the patches are restricted by the size of the grind-out. It is therefore necessary to verify if these dimensions will meet the minimal size requirements that are necessary to transfer the load out of the skin into the repair and back into the skin.

In order to verify the dimensions, the patch that is bonded into the grind-out is considered as a single sided supported repair. Since the grind-out is assumed not to have a crack in the remaining substrate, there will be only two transfer lengths necessary, one at each patch tip (see paragraph 2.5.3, Step 5). For C5033, one important restriction is that there is significant restraint against out-of-plane bending, which is the case here since that is one of the loading requirements for the simulated wing skin.

2.5.2 Materials Properties

The specimens are designed for room temperature RT, 25 degrees Celsius (77 degrees Fahrenheit). Table 5 shows the material properties for the specimen and patch materials. Table 6 shows the material properties for the adhesive.

Table 5: Material properties for specimen and patch materials

	Skin material 7075-T6 bare	Patch material 2024-T3 bare	Patch material 5521/F4 boron-epoxy (R.T. properties)
Young's Modulus, E MPa (ksi)	71700 (10399)	73100 (10602)	195000 (28282)
σ_{ult} MPa (ksi)	572 (82.96)	483 (70.05)	1520 (220.46)
σ_{yield} MPa (ksi)	503 (72.95)	345 MPa (50.04)	NA
Thickness, t mm (inch)	4.826 (0.19)	3.175 (0.125)	0.136 (0.00535) per ply
Thickness t for aluminum layer in hybrid patch mm (inch)	NA ^o	2.0 (0.08)	NA
Thickness of remaining substrate, $t_{substrate}$ mm (inch)	1.651 (0.065)	NA	NA
CTE per °C (per °F)	23.6×10^{-6} (13.11×10^{-6})	23.2×10^{-6} (12.89×10^{-6})	4.5×10^{-6} (2.5×10^{-6})

Table 6: Properties for adhesive Hysol EA 9696 0.06 psf (R.T. properties)

Plastic shear stress limit, τ_p MPa (ksi)	43.4 (6.295)
Shear Modulus, G MPa (ksi)	798 (115.7)
Cure temperature, T_{cure} °C (°F)	121 (250)
Glass transition temperature, T_g °Celsius (°F)	116 (241)
Effective temperature, T_{eff} °C (°F)	118 degrees Celsius (244 degrees Fahrenheit)
Elastic shear strain, γ_e	0.1*
Plastic shear strain, γ_p	0.5*
Ultimate shear strain, γ_{max}	0.6*
Thickness of cured adhesive layer, $t_{adhesive}$ mm (inch)	0.11 (0.0045)*
* Values for FM-73 0.06 psf, source: C5033 [4]	

2.5.3 Repair Design Process

Step 1: Load Determination

When designing a repair, it must be verified that the repair has sufficient load carrying capability. The repair is not allowed to fail at a static load with a magnitude of design ultimate load, DUL.

In case the DUL loads are unknown, CRMS requires the bond line to be able to carry the following load per unit width for through-thickness defects (WRALC/ENFA guideline):

$$P = UTS_{skin} \times t_{skin}$$

When basing the load carrying capacity on the material ultimate tensile strength, UTS, the repair will never be the weakest link and failure will never occur in the repaired area but outside the repaired area. Although very conservative, UTS_{skin} can be replaced by the highest load that the structure will ever see, which is DUL (design ultimate load).

As was mentioned in paragraph 2.5.1, the repair is assumed to carry the load that is normally carried by the removed material; the remaining substrate (the material that is left after making the grind-out) is still carrying part of the total load that is going through the repaired structure. Therefore, the load carrying capability is based on:

$$P = DUL_{structure} \times (t_{skin} - t_{substrate})$$

The stresses for which these repairs are verified are DUL of the spectrum loads, and are:

$$DUL_{tension} = 1.5 \times 115.8 \text{ MPa (16.8 ksi)} = 173.7 \text{ MPa (25.2 ksi)}$$

$$DUL_{compression} = 1.5 \times -193 \text{ MPa (-28 ksi)} = -289.5 \text{ MPa (-42 ksi)}$$

Resulting in the following loads per unit width:

$$P_{tension} = 551.5 \text{ N/mm}$$

$$P_{compression} = 919.2 \text{ N/mm}$$

Note that it does not matter for the adhesive whether the specimen is loaded in tension or compression (ignoring thermal residual tensile stresses), and therefore the $P_{compression}$ value will be used to verify the adhesive load carrying capability.

To verify the fatigue durability of the repairs, realistic spectrum tests will be performed, since the spectrum is available for this particular location (WS 320).

Step 2: Damage Tolerance Check

Another important requirement is that the unrepaired damage is not critical at Design Limit Load, DLL, and the inspection interval must be set such that the damage cannot grow to critical size before the next inspection is due. This is to assure that in case the bond line fails, the structure is still able to carry the required loads. Since the assumption is that there is no crack in the remaining substrate, this requirement means that at DLL, the maximum stress in the remaining material without the repair must be well under ultimate strength of the material, in this case:

$$7075-T6: \quad \sigma_{ult} = 572 \text{ MPa (82.96 ksi)}$$

$$\quad \sigma_{yield} = 503 \text{ MPa (72.95 ksi)}$$

$$7178-T6 \text{ (for the older aircraft):} \quad \sigma_{ult} = 607 \text{ MPa (88.04 ksi)}$$

$$\quad \sigma_{yield} = 538 \text{ MPa (78.03 ksi)}$$

$$E = 71700 \text{ MPa (10399 ksi) for both materials}$$

Source: www.matweb.com

When reducing the thickness by 2/3, the stress in the remaining substrate does not increase threefold. Since the grind-out acts as an inclusion that is less stiff, load will be bypassed around the grind-out, lowering the actual stress in the remaining material.

Static strain gage measurements [5] showed that the maximum stress (membrane plus bending) at an applied far field stress of 120 MPa (17.4 ksi) at the center of the unrepaired (double-taper) grind-out is 221 MPa (32.05 ksi). This is well below the maximum allowable stress, and therefore the DLL requirement is easily met.

Also note that even when the crack is taken into consideration (half crack size $a = 5.0 \text{ mm}$), the maximum stress intensity at the crack tip in the unrepaired (double-taper) grind-out would have been $27.7 \text{ MPa}\sqrt{\text{m}}$ ($25.2 \text{ ksi}\sqrt{\text{inch}}$) assuming a through the thickness crack in a finite width plate. This is well below the plane stress fracture toughness value for 7075-T6 (K_{Ic} is $79.0 \text{ MPa}\sqrt{\text{m}}$ / $71.9 \text{ ksi}\sqrt{\text{inch}}$ for 0.1" thick 7075-T6 sheet with buckling constraints).

Step 3: Patch Stiffness/Thickness

Before the in-plane repair dimensions can be verified, the thickness of the patch will have to be determined. Applying a repair that is too stiff will result in unwanted load attraction into the repaired area, possibly leading to problems at the patch tips. Initiating a crack at the run-out of the repair is a very dangerous situation that should be avoided. Applying a repair that is not stiff enough will allow for stresses in the grind-out region higher than desired, and could lead to crack nucleation in the substrate under the repair.

For repairing corrosion grind-outs where the remaining substrate is undamaged, the C5033 procedure is to restore the original extensional stiffness of the structure. However, the CRMS manual allows the stiffness ratio of the patch/substrate combination to be up to 1.5, following the accepted limits for external repairs of through-the-thickness damage.

This results in the following guideline:

$$\text{StiffnessRatio} : 1.0 \leq \frac{E_{\text{patch}} t_{\text{patch}} + E_{\text{substrate}} t_{\text{substrate}}}{E_{\text{skin}} t_{\text{skin}}} \leq 1.5$$

where $E t$ is known as the extensional stiffness

The following three flush repairs were used:

- Aluminum repair
- Boron-epoxy repair
- Hybrid repair: aluminum combined with boron-epoxy

The aluminum repairs were made out of 2024-T3 bare aluminum, with a thickness of 3.175 mm (0.125"). Since the removed material is replaced with material with similar thickness and Young's modulus, the stiffness ratio of the aluminum repair is 1.01.

The boron-epoxy repairs consisted of 13 plies of 5521/F4 boron-epoxy patch (Specialty Materials), ply thickness 0.136 mm (0.00535"). The stiffness ratio of the patch-substrate combination is 1.34.

The hybrid repairs consisted of 7 plies of 5521/F4 boron-epoxy and one layer of 2024-T3 bare aluminum with a thickness of 2 mm (0.08"). The stiffness ratio of the repair-substrate combination is 1.30.

Step 4: Patch Strength

The minimum patch strength per unit width must meet the following requirement according to CRMS and C5033:

$$UTS_{\text{patch}} \times t_{\text{patch}} \geq UTS_{\text{skin}} \times (t_{\text{skin}} - t_{\text{substrate}})$$

However, since the structure will never see UTS_{skin} , this requirement can be relaxed to:

$$UTS_{\text{patch}} \times t_{\text{patch}} \geq DUL_{\text{structure}} \times (t_{\text{skin}} - t_{\text{substrate}}) = 551.5 \text{ N/mm}$$

Notice that the $DUL_{\text{structure}}$ is DUL_{tension} from Step 1, which was 173.7 MPa

The strength per unit width for the three different repairs are:

1. The strength per unit width for the 2024-T3 aluminum patch:

$$483 \text{ MPa} \times 3.175 \text{ mm} = 1533.5 \text{ N/mm}$$

2. The strength per unit width for the boron patch:
1520 MPa x 13 plies x 0.136 mm = 2687.4 N/mm

3. The strength per unit width for the hybrid patch:
 $1520 \text{ MPa} \times 7 \text{ plies} \times 0.136 \text{ mm} = 1447 \text{ N/mm}$ for the boron-epoxy part
 Since boron-epoxy has a lower failure strain than aluminum 2024-T3, the patch will partially fail when the failure strain of the boron-epoxy has been reached. Assuming linear behavior for boron-epoxy up to failure results in a failure strain of 7.8×10^{-3} . The aluminum part of the patch will have deformed plastically at this strain level and the stress level will be approximately 330.95 MPa (48 ksi) [6]. Therefore, the load per unit width in the aluminum layer of the hybrid patch at the failure strain of the boron-epoxy will be $330.95 \text{ MPa} \times 2 \text{ mm} = 661.9 \text{ N/mm}$ for the aluminum part, resulting in a total strength per unit width of 2108.9 N/mm

Therefore, all the repairs that will be discussed in the next paragraph will meet the strength requirement.

Step 5: Patch Length

The length of the repair is based on the bond length that is required to transfer the load from the skin into the patch through the adhesive, also known as the transfer length. One transfer length consists of a plastic zone and an elastic zone. In the elastic zone, the shear stress is decreased from the plastic limit τ_p down to a value approaching zero, see Figure 13.

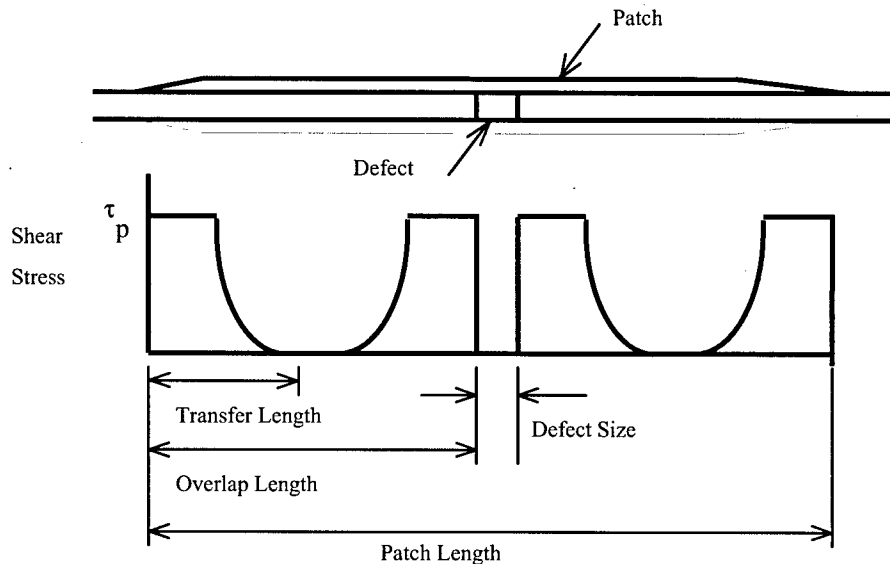


Figure 13: Relationship between transfer length, overlap length and patch length [C5033]

Since the assumption is that there is no crack in the remaining substrate (the material that is left after making the grind-out), there are only two transfer lengths necessary, one at each patch tip.

Since the assumption is that the remaining material is still carrying part of the total load, the load that will be transferred through the adhesive layer is based on the thickness of the removed material (3.175 mm) and the maximum $DUL_{compression}$ case (which was 289.5 MPa). Therefore the calculations are performed as if a 3.175 mm thick skin is repaired with a single-sided supported repair.

The plastic zone size l_p is calculated as follows [3]:

$$l_p = \frac{DUL_{compression} (t_{skin} - t_{substrate})}{2\tau_p} = 10.59 \text{ mm}$$

The elastic zone l_e size is defined by [3,4]:

$$l_e = \frac{3}{\lambda}$$

where [3]:

$$\lambda = \sqrt{\frac{G}{t_{adhesive} \left(\frac{1}{E_{skin} (t_{skin} - t_{substrate})} + \frac{1}{E_{patch} t_{patch}} \right)}}$$

Since the patch properties play a role in this equation, the elastic transfer lengths are different for the different patch materials:

- $l_e = 11.94$ mm for the aluminum repairs
- $l_e = 13.04$ mm for the boron-epoxy repairs
- $l_e = 12.94$ mm for the hybrid repairs

The transfer length $L_T = l_e + l_p$ becomes:

- $L_T = 22.53$ mm for the aluminum repair
- $L_T = 23.63$ mm for the boron-epoxy repair
- $L_T = 23.53$ mm for the hybrid repair

For a single-sided supported repair, the total patch length (including taper) is normally four times the transfer length. Note however that the repair of a corrosion grind-out where the patch is bonded into the grind-out, requires only 2 transfer lengths since no cracked substrate is assumed [4], therefore making the minimum required patch lengths:

- Minimum patch length = 45.06 mm for the aluminum repair
- Minimum patch length = 47.26 mm for the boron-epoxy repair
- Minimum patch length = 47.06 mm for the hybrid repair

For patches where the length of the required taper is less than l/λ , there is no need to add additional length to account for the taper [4]. The values for l/λ are:

- $l/\lambda = 3.98$ mm for the aluminum repair
- $l/\lambda = 4.35$ mm for the boron-epoxy repair
- $l/\lambda = 4.31$ mm for the hybrid repair

Since the taper in loading direction is 30 mm (determined by the T.O.), the difference between l/λ and the 30 mm must be added to each transfer length [4]. Since there are two transfer lengths necessary, the minimum patch lengths for the different materials become:

- Minimum patch length, accounted for taper = 97.1 mm for the aluminum repair
- Minimum patch length, accounted for taper = 98.56 mm for the boron-epoxy repair
- Minimum patch length, accounted for taper = 98.44 mm for the hybrid repair

Since the grind-out is 136 mm long and the patches fill up the entire grind-out, the minimum patch length requirement is met for all three different types of repair. Note however, that the patch dimensions will change for temperature cases other than room temperature (since the adhesive properties depend on temperature), and changes to the grind-out and the use of a thicker adhesive might become necessary.

Step 6: Adhesive Shear Strains

It must be verified that the maximum allowable shear strain in the adhesive is not exceeded. In case the adhesive remains elastic, the elastic shear strain follows from [3]:

$$\gamma_e = \frac{\sigma_{\text{underrepair}} t_{\text{substrate}} \lambda}{G}$$

where:

$$\lambda = \sqrt{\frac{G}{t_{\text{adhesive}}} \left(\frac{1}{E_{\text{skin}} (t_{\text{skin}} - t_{\text{substrate}})} + \frac{1}{E_{\text{patch}} t_{\text{patch}}} \right)}$$

$$\sigma_{\text{underrepair}} = \left(\frac{E_{\text{skin}} t_{\text{substrate}}}{E_{\text{patch}} t_{\text{patch}} + E_{\text{skin}} t_{\text{substrate}}} \right) \sigma_{\text{patchtip}}$$

$$\sigma_{\text{patchtip}} = \Omega \sigma_{\text{applied}} + \left[E_{\text{skin}} \left(\left(CTE_{\text{patch}} - CTE_{\text{effskin}} \right) (RT - T_{\text{eff}}) + \left(CTE_{\text{patch}} - CTE_{\text{skin}} \right) (T_{\text{oper}} - RT) \right) \right]$$

In which Ω is the load inclusion factor, which depends on both the aspect ratio and stiffness ratio of the repair. Ω is approximately 1.2 for the aluminum repair and approximately 1.22 for the boron and the hybrid repairs.

Since the entire specimen is heated up when curing the adhesive, the specimens are free to expand and therefore the $CTE_{effskin}$ is identical to the CTE_{skin} . Also, since the tests are performed in laboratory air, the operating temperature T_{oper} can be set at room temperature.

The applied stress $\sigma_{applied}$ is $DUL_{compression}$, which is 289.5 MPa in compression. The fact that this load is in compression is important since it will add to the compressive residual thermal stresses at the patch tip caused by the mismatch in CTE between the patch and the skin material.

The effective temperature at which the adhesive starts to build up thermal residual stresses is the average of the cure temperature T_{cure} and the glass transition temperature T_g :

$$T_{eff} = \frac{(T_{cure} + T_g)}{2}$$

In case the adhesive becomes plastic, the plastic shear strain follows from:

$$\gamma_p = \frac{\tau_p}{2G} \left(1 + \left(\frac{\sigma_{underrepair} t_{substrate} \lambda}{\tau_p} \right)^2 \right)$$

The shear strain limits for the adhesive at RT are:

$$\begin{aligned} \gamma_{e \text{ allowable}} &= 0.1 \\ \gamma_{p \text{ allowable}} &= 0.5 \\ \gamma_{max \text{ allowable}} &= 0.6 \end{aligned}$$

According to C5033, the margin of safety (MOS) according to the following equation must be 0.2 or higher:

$$MOS = \frac{(\gamma_{e \text{ allowable}} + \gamma_{p \text{ allowable}})}{\gamma_{calculated}} - 1$$

Now that all variables are known, the strain values can be calculated for the different repairs:

$$\begin{aligned} \text{Aluminum repair:} & \quad \gamma_e = 0.06 \\ \text{Boron-epoxy repair:} & \quad \gamma_e = 0.06 \\ \text{Hybrid repair:} & \quad \gamma_e = 0.05 \end{aligned}$$

Calculating the MOS results in a factor of 9, and therefore easily meets this requirement.

2.6 Repairs

As was shown in the previous paragraphs, all three repairs that are used meet the CRMS and C5033 requirements under the test conditions. This paragraph will give more detail on each specific repair.

2.6.1 Aluminum Repair

Using an aluminum repair has the following advantages and disadvantages:

Advantages:

- No, or limited thermal residual stresses after bonding the patch
- Rivets can be countersunk through the patch

Disadvantages:

- The extensional stiffness of the repair is limited by the flushness requirement. Only the extensional stiffness of the removed material can be replaced
- Crack nucleation in the patch is a possible failure mode
- Patch has to be the perfect positive of the grind-out
- Patch needs surface preparation similar to skin before bonding

The aluminum repairs that were used were made of 2024-T3 bare aluminum, with a thickness of 3.175 mm (0.125"). The aluminum repair is used in combination with the pyramid shaped grind-out (taper in two directions). Both the patch and grind-out were made using CNC (computer numerically controlled) milling equipment and therefore the patch was the exact positive of the grind-out.

Since the removed material is replaced with material with similar thickness and Young's modulus, the stiffness ratio of the aluminum repair is 1.01. Figure 14 shows the specimen before and after bonding of the aluminum patch. As can be seen, the rivets have been re-countersunk through the repair.

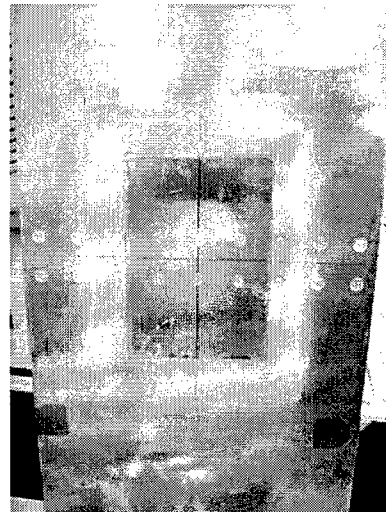
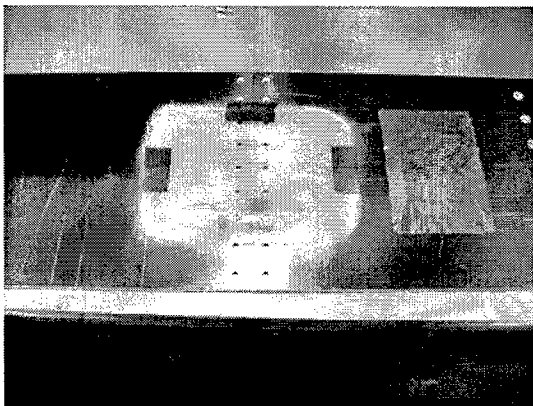


Figure 14: Aluminum repair before and after bonding

2.6.2 Boron-Epoxy Repair

Using a boron-epoxy repair has the following advantages and disadvantages:

Advantages:

- Higher Young's modulus allows for a higher stiffness ratio within in the grind-out
- Co-curing the patch makes it easier to get a good fit in the grind-out
- No patch cracking issues

Disadvantages:

- Thermal residual stresses after bonding, and due to thermal cycling in service
- Potential compression problems with boron-epoxy patches
- Potential issues with fasteners through the patch, fibers will be cut

The boron-epoxy repairs consisted of the following:

- 13 plies of 5521/F4 boron-epoxy patch (Specialty Materials), ply thickness 0.136 mm (0.005")
- The stiffness ratio of the patch-substrate combination was 1.34.
- This repair was used in combination with the grind-out with only taper in loading direction. The patch follows the linear taper of the grind-out.
- The lay-up was uni-directional, inverted wedding cake, where the shortest ply is 76.2 mm (3") long and the longest ply is 136 mm (5.35")
- The hi-loks were countersunk at the bottom of the grind-out, after which the boron was bonded over the fasteners.

Figure 15 shows the repair after bonding.

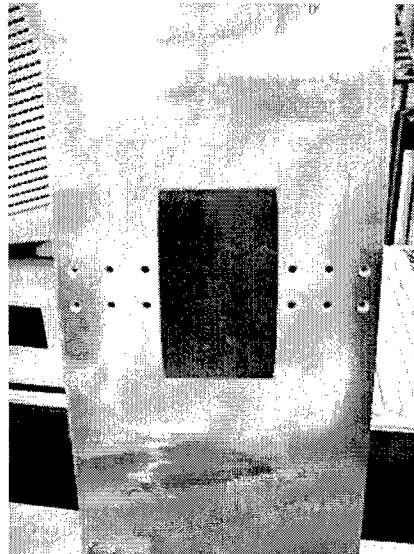


Figure 15: Boron-epoxy repair after bonding

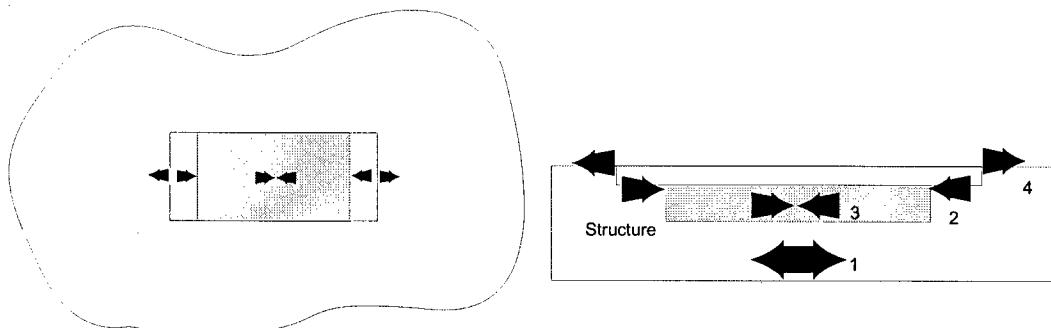
2.6.3 Hybrid Repair

Research in the past has shown that the application of boron-epoxy patches in a compression dominated situation can lead to possible disbonding [7,8], starting at the patch tip. This is due to a significant CTE (coefficient of thermal expansion) mismatch between the repair material and aluminum structure. Using a high temperature curing adhesive will result in a thermal residual stress state at the patch run-out that is compressive, whereas the thermal residual stresses at the center of the patch will be tensile. Adding mechanical compressive loading to this thermal residual stress state can therefore lead to disbonding of the patch or delamination within the patch itself, starting at the patch tips.

When using a patch material with a higher CTE than the effective CTE of the repaired structure, for example aluminum, the result will be residual thermal tensile stresses at the patch tip and residual thermal compressive stresses in the structure under the repair. The tensile stresses at the patch tip are beneficial when the dominant loading condition is compression, but the residual thermal compression in the structure under the repair will now be additional to the mechanical compression loading.

The idea of using a hybrid patch is not to develop a new material by creating an average CTE through the thickness of the entire patch, but to separate the most critical areas in the repair by extending one layer of the repair beyond the other layers, and therefore isolating the residual thermal effects in the critical areas from each other.

By combining the best properties of both aluminum and boron-epoxy in the form of a hybrid patch, it is possible to create beneficial residual thermal stresses at both the patch tip and in the structure under the repair. Figure 16 [9] shows the residual thermal stress state for a hybrid patch concept that is beneficial for a compression dominated loading condition. The arrows do not imply externally applied loads, only thermal residual stresses.



- White layer is aluminum
- Gray layer is boron-epoxy

Figure 16: Hybrid patch concept for a compression dominated structure

In the case of a compression dominated loading situation the aluminum layer extends beyond the boron-epoxy layer. Since the effective CTE of the structure is lower than the free CTE of the aluminum layer of the patch, the aluminum layer will locally create residual thermal tensile stresses at the patch tip (location 4) in the structure, which are beneficial when the structure is predominantly loaded in compression. The residual thermal tensile stresses at location 4 can be deducted from the mechanically applied compressive loads, therefore reducing the problems of patch tip disbonding. Note however that there will still be compressive stresses in location 2, at the tip of the boron layer of the patch. These stresses however will be significantly lower than for the case where the entire patch is made out of boron, since the total residual thermal stresses are lower (because less boron was used), and because part of the load will stay in the aluminum layer of the repair instead of being transferred into the boron part of the patch.

Depending on the ratio of boron and aluminum in the patch, the residual thermal stress state in the structure under the repair will be tensile or compressive. In the case the overall CTE of the hybrid patch is lower than the effective CTE of the structure; the residual thermal stress state will be tensile in the structure under the repair. In the case the overall CTE of the hybrid patch is higher than the effective CTE of the structure; the residual thermal stress state will be compressive in the structure. For the hybrid repairs used here, where the entire specimen is heated during cure, the residual thermal stresses in the specimen under the repair will be tensile.

Another big advantage of the hybrid concept is that by first bonding the boron-epoxy plies to the substrate (bottom of the grind-out), it is more difficult for a possible crack in the substrate to grow into the aluminum layer of the patch (fiber-metal laminate principle).

To summarize, using a boron-epoxy/aluminum hybrid repair has the following advantages and disadvantages:

Advantages:

- Higher Young's modulus of the two combined materials allows for a higher stiffness ratio within in the grind-out
- No patch cracking issues (Fiber Metal Laminates principle)
- Possibility to locally tailor the thermal stresses to obtain the most beneficial stress situation
- Fasteners through patch might be possible

Disadvantages:

- Slightly more complicated
- Potential issues with fasteners through the patch, fibers will be cut

The hybrid repairs consisted of the following:

- 7 plies of 5521/F4 boron-epoxy, shortest ply is 76.2 mm (3"), longest ply is 94 mm (3.7"), taper ratio of 1:10, ply thickness 0.136 mm (0.005")
- 1 top layer of 2024-T3 bare aluminum with a thickness of 2 mm (0.08")
- The taper followed the linear taper of the grind-out
- Hi-Loks countersunk at the bottom of grind-out
- Stiffness ratio of the repair-substrate combination is 1.30

The boron-epoxy part of the patch is bonded to the substrate using one adhesive layer of Hysol EA9696 0.06 lbs/ft². The aluminum top layer of the patch is bonded to the boron-epoxy/aluminum substrate using the same adhesive. The combined thickness of all these layers filled up the grind-out depth completely. Figure 17 through Figure 19 show the hybrid repair before and after bonding.

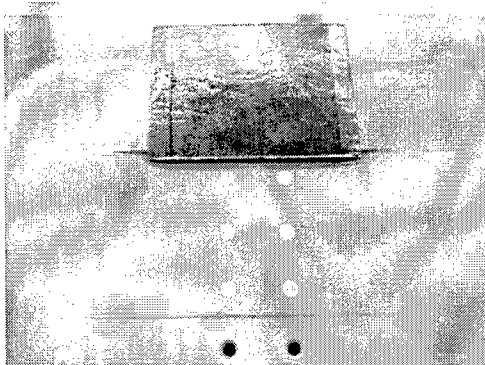


Figure 17: Boron-epoxy plies of the patch with one layer of EA9696 adhesive. Note the hi-loks at the bottom of the grind-out

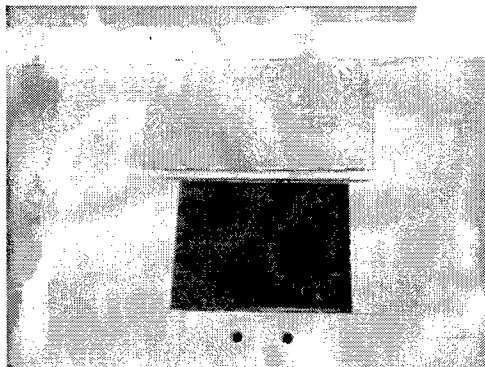


Figure 18: Boron-epoxy plies at bottom of grind-out, aluminum ply with EA9696 adhesive ready to be fitted. Note that the aluminum layer is longer than the boron-epoxy.

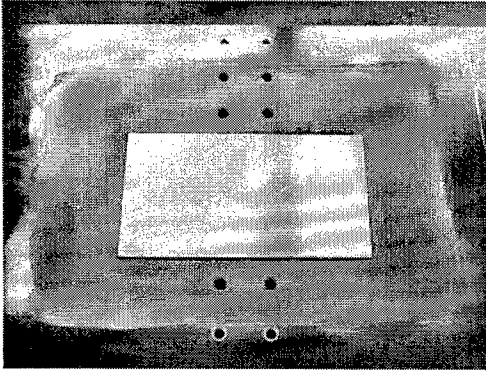


Figure 19: Hybrid patch installed

2.7 Surface Preparation and Bonding

Before the repairs can be bonded to the specimens, all aluminum bonding surfaces, specimen, aluminum patch and aluminum part of hybrid patch, must be surface prepped.

The aluminum parts were surface prepped using the Sol-Gel surface preparation procedure. This procedure involves the following steps:

- Degrease using Acetone
- Removal of old oxide layer using 3M Scotch-Brite Grade A (very fine) discs
- Degrease using Acetone
- Gritblast using compressed oil free nitrogen and 50 micron aluminum oxide (virgin grain)
- Wet the surface for at least 3 minutes using Sol-Gel AC-130 (Advanced Chemistry and Technology, Inc.)
- Air dry for 30 minutes
- Apply Cytec BR6747-1 water based primer
- Air dry for 30 minutes
- Cure for 1 hour at 121°C (250°F)

After all the bonding surfaces had been cured, they could be stored until bonding at a later time. The adhesive that was used for all bonding was Hysol EA9696 epoxy film adhesive, with a specific weight of 0.06 lbs/ft².

To simulate in-field bonding conditions, all bonding was performed with only vacuum pressure and a 121°C (250°F) cure cycle. The cure cycle is as follows:

- Apply full vacuum pressure (maximum of approximately 23" Hg at 7000 ft altitude USAFA)
- Ramp up temperature between 0.6 and 5.6 °C per minute (1.08 to 10.08 °F per minute), to 60°C (140°F)
- Hold at 60°C (140°F) for 15 minutes to allow air to be evacuated
- Decrease vacuum level to 14" Hg to avoid the formation of voids in the bond line
- Ramp up temperature between 0.6 and 5.6°C per minute, to 121°C (250°F)
- Hold at 121°C (250°F) for 90 minutes
- Decrease temperature between 0.6 and 5.6°C per minute (1.08 to 10.08 °F per minute), do not remove vacuum until part temperature is below 50°C (122°F)

Bonding was done using a Heatcon vacuum table, see Figure 20 and Figure 21. The boron-epoxy and hybrid patches were co-cured during the adhesive cure-cycle.

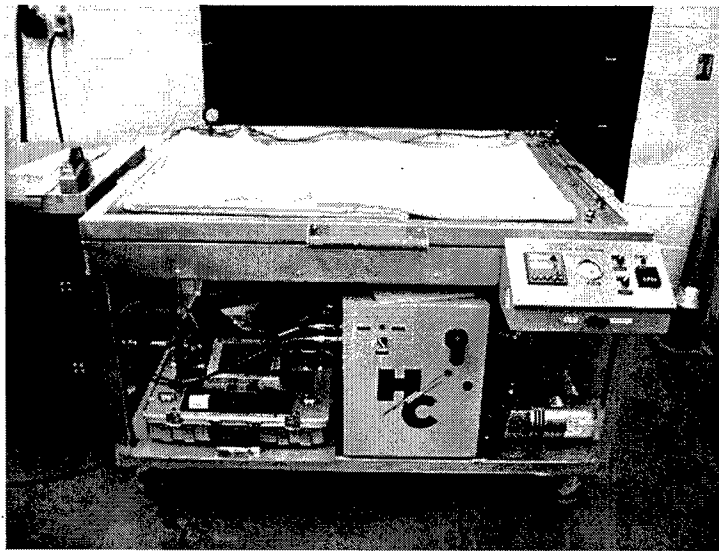


Figure 20: Heatcon vacuum table

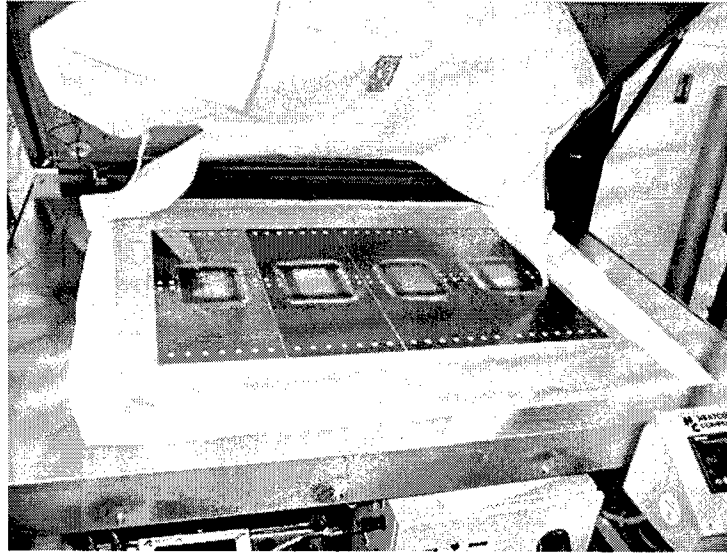


Figure 21: Specimen with aluminum repairs in vacuum table

3. Fatigue Testing

3.1 Test Procedure

In order to determine the most efficient and durable type of repair, crack growth rates under the repairs were studied. Crack growth rates will give valuable information on the stress state under the bonded repair. If no crack would be present one would be looking at a possible crack nucleation event, which typically has large amounts of scatter.

Note that the repairs were not designed with a crack in the substrate (the substrate was assumed to be undamaged) but the crack growth rates will be a good measure of how the different types of repairs perform relatively to each other. Also, testing the repairs in fatigue will give a good insight in the durability of the repairs under spectrum loading and could bring to light other failure modes such as patch tip failures, crack initiation in the patches, or disbonding or delaminations in the repairs.

Since the starter crack was covered by the repair, and the backside of the crack was covered by the 1 mm (0.04") thick half sheet, a Staveley eddy current NDI was used to measure crack growth. Measurements were taken from the backside of the repair through the 1 mm thick half sheet. The eddy current measurement does not necessarily give the exact same crack size as the optical measurement that was done during pre-cracking but will give the change in crack length during the test by identifying the location of the crack tip with each measurement. Since the initial and final crack sizes are known from optical measurements, the eddy current measurements can be easily corrected. Whenever the specimen had to be disassembled for c-scanning of the repair, the crack measurements were optically verified. Eddy current proved to be an accurate method for determining the crack growth without the need for removal of the fasteners and thin sheet.

Since disbonds and delaminations were a concern during the compression loading, specimens were taken out of the test frame at regular intervals, disassembled and c-scanned (Figure 22) to look for any signs of disbonding.

Testing was done using a MTS 810 110 kip (Figure 23) and 55 kip test frame, running TestStar IIs and TestStar IIm. The constant amplitude tests were tested at a frequency of 4 Hz, the spectrum testing was ramp rate controlled at 250 kN/sec. Humidity and temperature were monitored during testing.

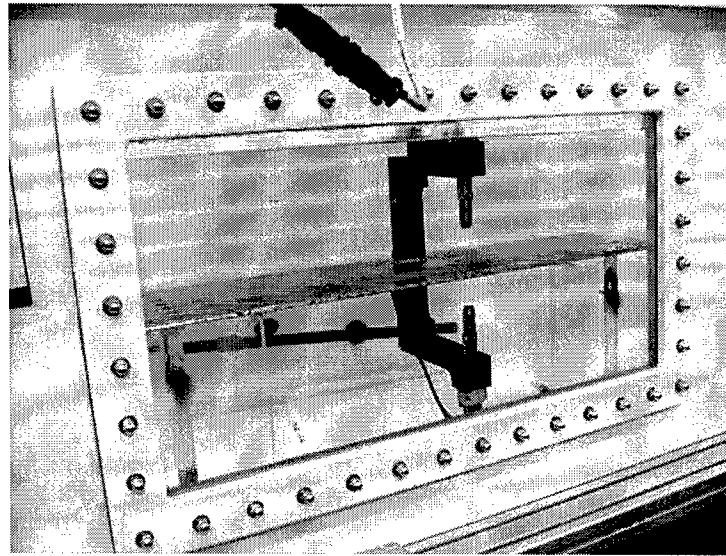


Figure 22: Specimen with bonded repair in c-scan tank

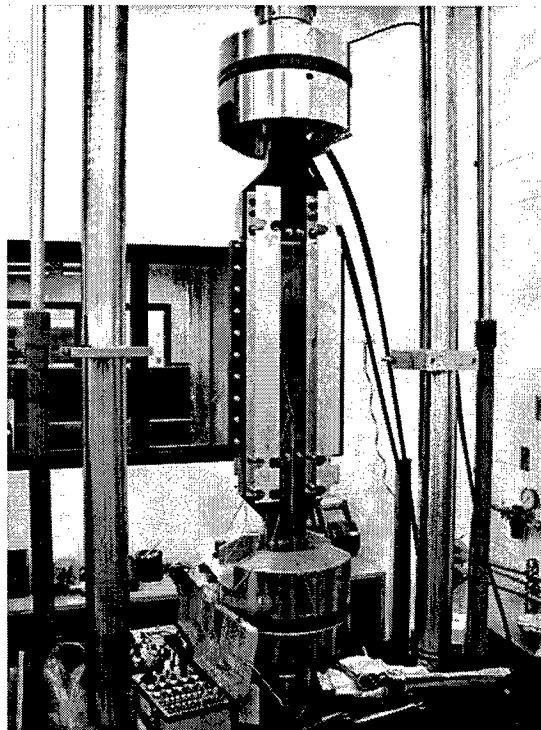


Figure 23: MTS 810 110 kip hydraulic load frame

3.2 Test Matrix

Table 7 and Table 8 show the specimens that were tested. As can be seen, the testing was split up in a constant amplitude part and a spectrum test part.

The constant amplitude testing was split up in a tension and compression part:

- Tension load of 120 MPa (17.4 ksi), R=0.05 to determine the repair with the best crack stopping capability. Since no tensile load in the spectrum was over 115.8 MPa (16.8 ksi), using this load should be very conservative and makes it possible to compare the results to other CASTLE test data from the past.
- Compression load of -150 MPa (-21.8 ksi), R=0.05 to determine if disbonds or delaminations are a problem. The spectrum has only 278 valleys that are below -150 MPa (out of 937,441 segments per full spectrum block, 10 blocks per life time).

Spectrum fatigue testing:

- Spectrum testing was done to verify the performance under realistic fatigue loading and to check for unexpected failure modes
- Maximum tensile stress of 115.8 MPa (16.8 ksi)
- Maximum compressive stress of -193 MPa (-28 ksi)
- Although only twice the remaining life time has to be tested, two life times were tested.
- A truncated spectrum was used to reduce test time. The spectrum is normalized such that the maximum in tension is 1.0. Truncation was 10% on positive peak-valley pairs and 25% on the negative peak-valley pairs

Table 7: Constant Amplitude Test Specimens

Specimen Number	Repair Type	Loading Type	Maximum Stress Level MPa (ksi) and R-ratio
CA1	No Repair	Tension	120 (17.4), R=0.05
CA2	No Repair	Tension	120 (17.4), R=0.05
CA3	No Repair	Tension	120 (17.4), R=0.05
CA4	No Repair	Tension	120 (17.4), R=0.05
CA5	Aluminum Patch	Tension	120 (17.4), R=0.05
CA6	Aluminum Patch	Tension	120 (17.4), R=0.05
CA7	Aluminum Patch	Tension	120 (17.4), R=0.05
CA8	Aluminum Patch	Tension	120 (17.4), R=0.05
CA9	Boron-epoxy Patch	Tension	120 (17.4), R=0.05
CA10	Boron-epoxy Patch	Tension	120 (17.4), R=0.05
CA11	Boron-epoxy Patch	Tension	120 (17.4), R=0.05
CA12	Boron-epoxy Patch	Tension	120 (17.4), R=0.05
CA13	Hybrid Patch	Tension	120 (17.4), R=0.05
CA14	Hybrid Patch	Tension	120 (17.4), R=0.05
CA15	Hybrid Patch	Tension	120 (17.4), R=0.05
CA16	Hybrid Patch	Tension	120 (17.4), R=0.05
CA17	Aluminum Patch	Compression	-150 (-21.8), R=0.05
CA18	Aluminum Patch	Compression	-150 (-21.8), R=0.05
CA19	Boron-epoxy Patch	Compression	-150 (-21.8), R=0.05
CA20	Boron-epoxy Patch	Compression	-150 (-21.8), R=0.05
CA21	Hybrid Patch	Compression	-150 (-21.8), R=0.05
CA22	Hybrid Patch	Compression	-150 (-21.8), R=0.05

Table 8: Spectrum Test Specimens

Specimen Number	Repair Type	Normalized Stress in Spectrum MPa (ksi)
S1	No Repair	1.0=115.8 (16.8)
S2	No Repair	1.0=115.8 (16.8)
S3	Aluminum Patch	1.0=115.8 (16.8)
S4	Aluminum Patch	1.0=115.8 (16.8)
S5	Aluminum Patch	1.0=115.8 (16.8)
S6	Boron-epoxy Patch	1.0=115.8 (16.8)
S7	Boron-epoxy Patch	1.0=115.8 (16.8)
S8	Hybrid Patch	1.0=115.8 (16.8)
S9	Hybrid Patch	1.0=115.8 (16.8)
S10	Hybrid Patch	1.0=115.8 (16.8)

4. Test Results and Discussion

4.1 CA Tension Tests

Figures 24 through 27 show crack growth curves for the specimens tested under constant amplitude fatigue loading. Figure 28 shows a comparison of an unrepaired specimen and the three different types of repairs (the data of the most "average" specimen is shown for each type of specimen). More detailed crack growth data can be found in appendix A.

4.1.1 Specimens without Repairs

As can be seen from Figure 24, the unrepaired specimen showed rapid crack growth. Specimen CA1 had one of the crack tips link up to the adjacent rivet hole within the first measurement interval, which was initially set at 5000 cycles. After finishing specimen CA1 the intervals were reduced to 1000 cycles. Specimen CA4 linked up both crack tips at 7000 cycles. Testing of specimens CA2 and CA3 was stopped before the cracks could extend to the adjacent fastener holes.

4.1.2 Specimens with Aluminum Repairs

Figure 25 shows the crack growth curves for the four specimens with aluminum repairs tested in CA tension. Figure 28 shows that, although the aluminum repair has a stiffness ratio that is too low (below the desired stiffness ratio of 1.0) now that the remaining substrate is cracked, the aluminum repairs extended the fatigue life of the specimen significantly when compared to the unrepaired situation.

None of the specimens showed link-up to the adjacent rivet holes and the tests were stopped when the half crack size was approximately 12 mm. After this point it is not possible to use eddy current since the measurement will be affected by the influence of the adjacent rivet hole (the eddy current probe has a diameter of 8 mm).

Specimen CA5 did not show crack growth re-initiation within the first 10000 cycles. Although the pre-cracks were formed at a very low stress level (and therefore a very low stress intensity factor), the repair reduces the stress intensity so much that it did not start growing right away.

When looking at the data in appendix A.2, it can be seen that the symmetry of crack growth for the left and right crack tips (measured from the vertical centerline of the specimen) is acceptable. ASTM E647 [10] states that the left and right crack length should not differ more than 0.025 times the width of the panel, which is in this case 5.72 mm. All crack growth data falls within this requirement.

However, it must be noted that it is debatable whether this requirement should not be met with respect to the width of the grind-out instead of the panel width, since asymmetry in crack growth could be affected by the crack growing towards the edge of the grind-out. When taking the smallest grind-out width of 62 mm, the allowable difference between the left and right crack tip would be reduced to 1.55 mm. Specimen CA7 would be the only specimen that falls outside this limit.

None of the aluminum repairs showed any crack nucleation in the repair itself (helped by the fact that the patches were made out of 2024-T3), nor did any of the rivet holes other than the test hole in the specimen show any sign of crack nucleation. This is important since cracking at any of the other locations would change the load transfer through the thin sheet into the specimen.

C-scans were made of all specimens after completion of the tests (see appendix B.1) and none of the repairs showed any signs of disbonding. This was not expected for the aluminum repairs but is important to verify.

4.1.3 Specimens with Boron-Epoxy Repairs

Figure 26 shows the crack growth curves for the four specimens with boron-epoxy repairs. Figure 28 shows that the boron-epoxy repair easily outperforms the aluminum repair. The benefit of the higher stiffness ratio of the boron-epoxy repair outweighs the disadvantage of the higher residual thermal stresses.

As can be seen from Figure 26, the cracks grow very slow in the beginning of the test, due to the high stress reduction under the repair. Some scatter can be seen but most is due to the differences in the early phase of the tests. No unexpected failure modes were seen during the tests. None of the rivet holes other than the test hole showed signs of crack nucleation.

From previous experience it was not expected that tension testing would show disbonding or delaminations. Unfortunately, it was not possible to make c-scans of the repairs before bonding due to equipment failure, but c-scans were made of all specimens after completion of the tests (appendix B.4) and confirmed that none of the repairs showed any signs of unexpected disbonding (adhesive failure) or delaminations (interlaminar failure).

The ultrasonic c-scans show some signs of air pockets around the fasteners, possibly air that was entrapped during the lay-up of the 13 plies. Another possibility however is that some air was drawn through the patch and through the fastener holes in the remaining substrate, although the hi-loks were tightened in the rivet holes. This air could then have expanded when the temperature increased during the cure cycle, leaving the voids.

Air pockets around the fasteners were less pronounced for the aluminum and hybrid repairs, which could be caused by the fact that for those two repairs the top layer is aluminum, which is impermeable to air, making it more difficult to draw air through the rivet holes. However, the air impermeability could also prevent the evacuation of air that is entrapped under the aluminum top ply.

When looking at the data in appendix A.3, it can be seen that the symmetry of crack growth for the left and right crack tips is acceptable when following ASTM E647. All crack growth data falls within the ASTM requirement. However, in case the width of the grind-out would be considered, 76.2 mm for the boron repairs, the allowable difference between the left and right crack tip would be reduced to 1.91 mm. Specimens CA9 and CA12 would fall outside this limit, the other two specimens meet this limit except for the final data points.

4.1.4 Specimens with Hybrid Repairs

Figure 27 shows the crack growth curves for the hybrid repairs. Figure 28 shows the performance of the hybrid repairs compared to the other repair types.

As can be seen in Figure 28, the hybrid repairs perform better than the aluminum repair. Despite the fact that the thermal residual tensile stresses under the boron-epoxy repairs are higher than for the hybrid repairs, the hybrid repair performs similar or slightly below the boron-epoxy repair. This can be explained by the fact that the hybrid patch is thicker than the boron patch. The advantage of a smaller CTE mismatch for the hybrid patch is counteracted by shear lag in the thicker hybrid patch, which is most noticeable in the absence of bending [11].

C-scans were made of all specimens before and after completion of the tests and none of the repairs showed any signs of disbonding or delaminations. There were limited air pockets around the fastener holes, but less significant than for the boron-epoxy repairs. The size and shape of these air pockets did not change during the tests.

Appendix A.4 shows that the symmetry of crack growth for the left and right crack tips is acceptable according to ASTM E647. However, changing to the width of the grind-out, 76.2 mm, the allowable difference between the left and right crack tip would be reduced to 1.91 mm. A few data points of specimen CA16 would fall outside this limit.

None of the hybrid repairs showed any crack nucleation in the aluminum top layer or in the specimen at the patch tip. None of the rivet holes, other than the test hole, showed signs of crack nucleation.

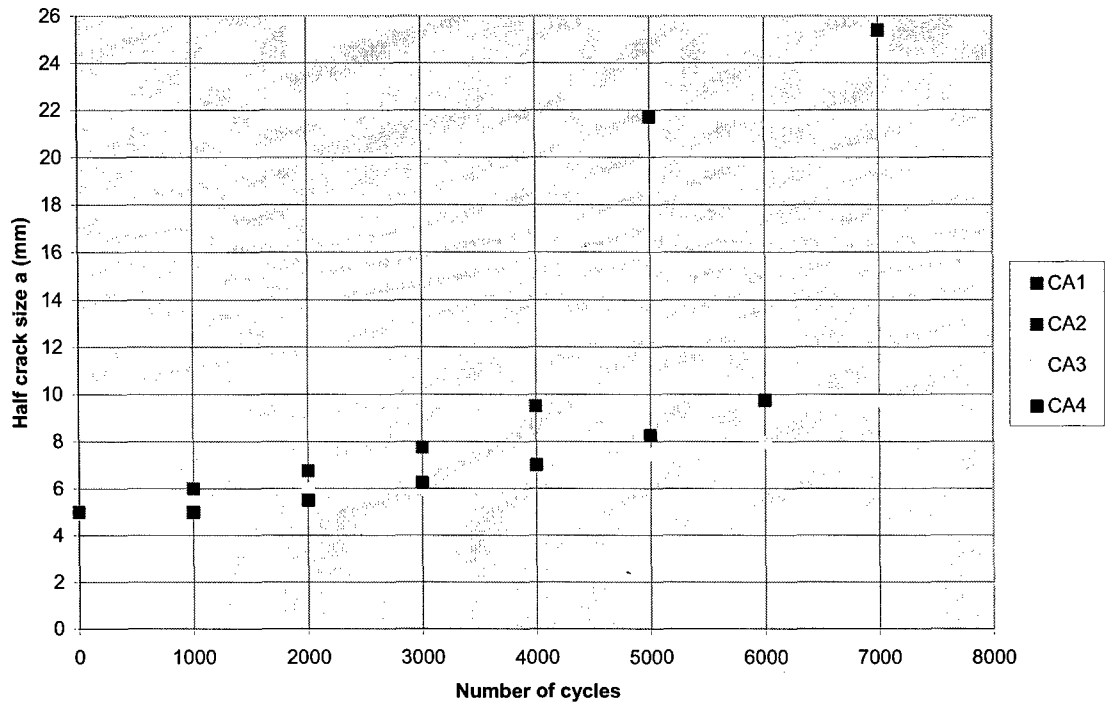


Figure 24: Specimens without repair, CA loading

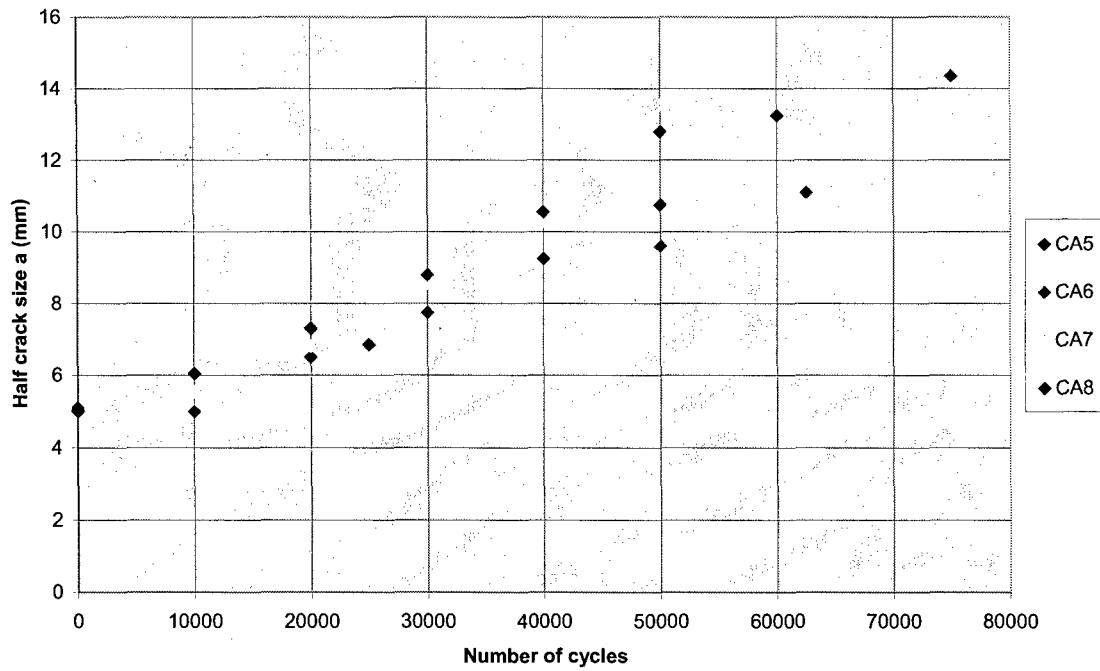


Figure 25: Specimens with aluminum repairs, CA loading

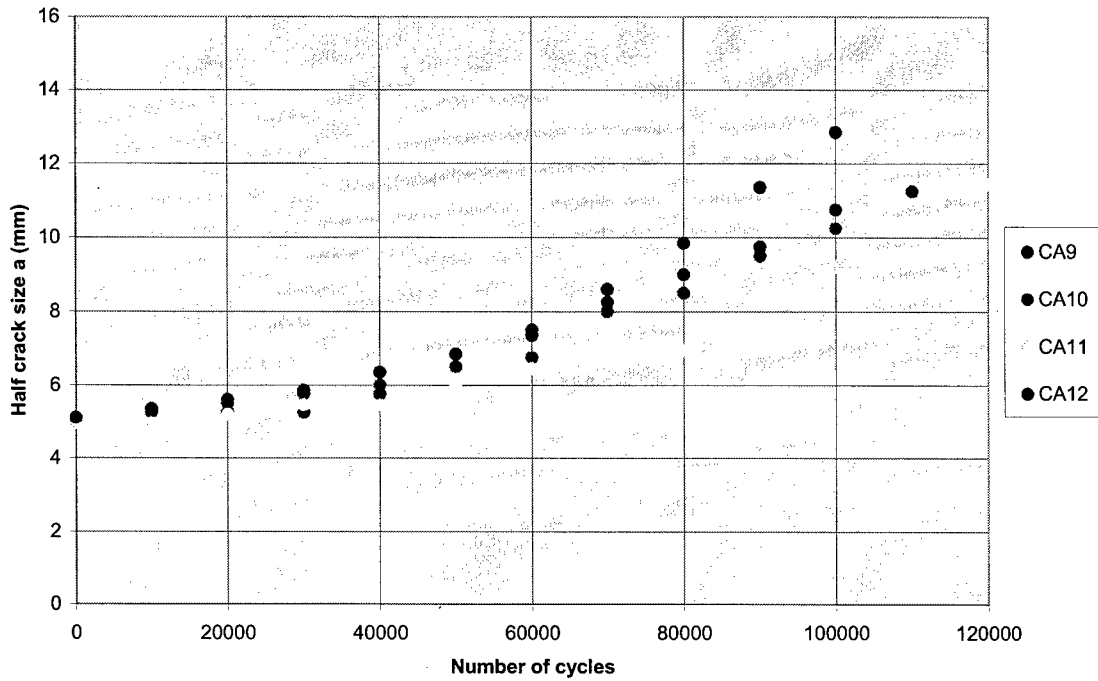


Figure 26: Specimens with boron-epoxy repairs, CA loading

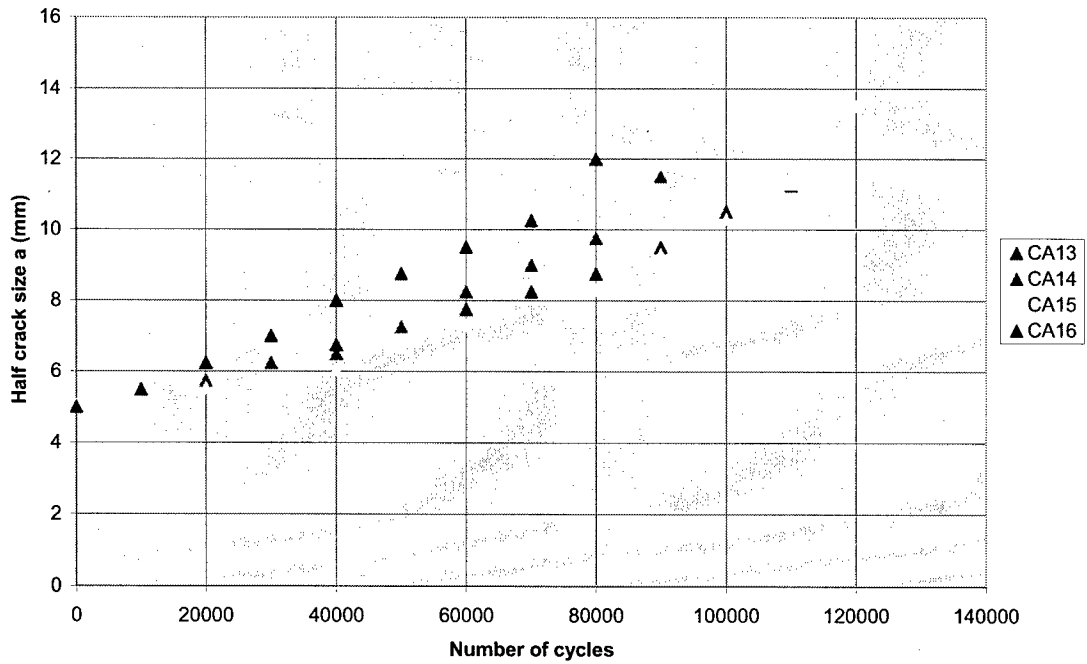


Figure 27: Specimens with hybrid repairs, CA loading

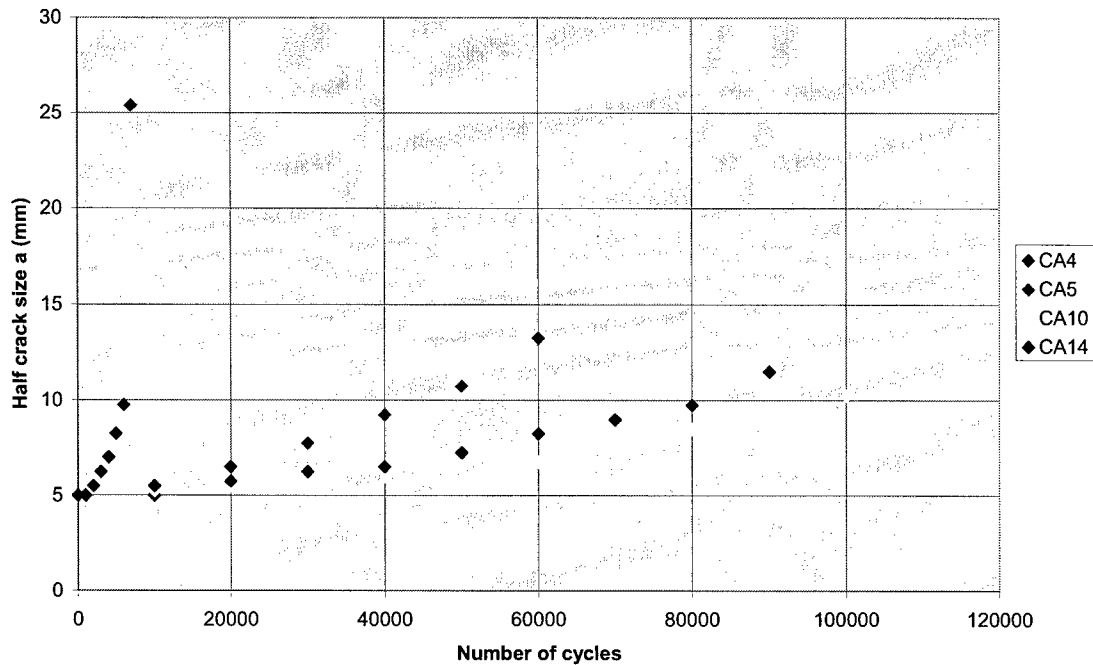


Figure 28: Crack growth curves for specimens with and without repairs, CA loading

4.2 CA Compression Tests

Two panels of each repair type were tested in compression, -150 MPa as the maximum compressive stress, $R=0.05$, for 1.5 million cycles at 4 Hz. The total test time was almost 5 days per specimen, excluding inspection time.

Specimens with aluminum repairs showed no disbonding after 1.5 million compression cycles (see appendix B.2) and no crack growth was observed for these specimens.

Crack growth while loading the specimen in compression without bending can only be expected when there are thermal residual stresses in the specimen. Since the panels were bonded using a vacuum table, the entire specimen was heated and therefore there should be no thermal residual stresses in the specimens with aluminum repairs.

Note that this situation can change for an on-aircraft repair where the structure is only locally heated. The cold surrounding structure will act as a restraint for the locally heated part of the structure, resulting in a lower effective CTE. When applying an aluminum repair in this situation, there will be compressive residual thermal stresses in the skin at the center of the repair, and residual thermal tensile stresses in the skin at the patch tips, which will be beneficial for a compression dominated loading condition.

C-scanning the hybrid repairs after 1.5 million compression cycles showed no signs of disbonding or delaminations, see appendix B.8.

Both the hybrid and boron-epoxy repairs showed crack growth after being loaded in compression. This is due to the residual thermal tensile stresses being cycled between their

maximum value, present after curing, and their minimum level, at the maximum applied compressive load. The crack growth that was observed for both repair types was significantly smaller than for the tension CA tests but nevertheless significant. There is not sufficient crack growth data available though to determine exact crack growth rates.

When c-scanning the boron-epoxy repairs, one of the repairs showed delaminations after as early as 250,000 cycles, the second specimen showed disbonding after 500,000 cycles, see appendix B.5. Figure 29 shows an example of a c-scan for a boron-epoxy repair before and after testing. As can be clearly seen, more than half the patch has disbonded. It may be clear that this is a very unwanted failure mode, which would not have been noted in a static test.

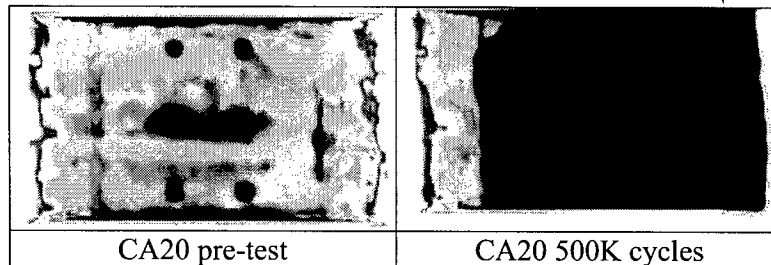


Figure 29: C-Scan of boron-epoxy repair before and after compression test

Figure 30 shows a photo of specimen CA20 after compression testing. Although already partially disbonded, the patch had to be peeled off before this photo could be taken. As can be seen from the photo, the bond line has failed between the adhesive and the boron-epoxy, in the resin-rich interface. All of the adhesive is on the aluminum specimen and the boron-epoxy has hardly any adhesive on it. Normally, an adhesion failure mode like this points towards poor surface preparation. However, remember that the boron-epoxy was co-cured and there is no surface preparation involved on the boron-epoxy side of the bond line. The fact that this specific interface failed is in itself not surprising, considering that this interface is the highest loaded interface of the repair. Since the film adhesive has superior properties compared to the epoxy in the boron pre-preg, the resin-rich part is most likely to fail.

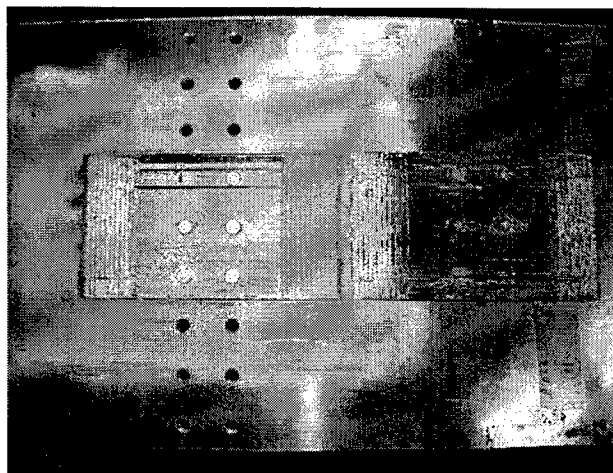


Figure 30: Boron-epoxy patch after compression test

4.3 Spectrum Tests

Table 6 shows the specimens that were tested under spectrum loading. Figures 31 through Figure 34 show the crack growth curves for the unrepaired specimens and the three different types of repairs. Figure 35 shows a comparison of the different types of repair, and Figure 36 shows the same curves as Figure 35 but now with the unrepaired specimen included.

Figure 31 shows the results for two unrepaired specimens. As can be seen, cracks did grow significantly when loaded using the upper wing skin spectrum, with pre-existing damage. For specimen S2, the crack linked up to the adjacent rivet holes within four spectrum passes, or 0.4 life time. Specimen S1 also linked up to the adjacent rivet holes within one life time.

Figure 32 shows that the aluminum repair performed very well under spectrum loading. Crack growth was reduced significantly compared to the unrepaired specimens. The difference between the aluminum repair and the hybrid repair is slightly smaller to what was seen in the results from the constant amplitude fatigue tests. It appears that the aluminum is benefiting from the lack of thermal residual stresses, the cracks under the aluminum repairs do not grow while loaded in compression. However, crack growth is still very minimal considering that two life times were tested, and keep in mind that only twice the remaining life time of the aircraft has to be demonstrated. Also, the assumption is that no crack is present when the repair is bonded into the grind-out. The aluminum repair showed no signs of unexpected failure modes, such as crack nucleation in the patch itself or in the specimen at the patch tip, or disbonding, see appendix B.3. There was also no sign of crack initiation in any of the other rivet holes under the repairs.

Specimens with boron-epoxy repairs showed crack growth that was irregular, see Figure 33. Delaminations were found between 1.2 and 1.6 life times, see appendix B.6. They were initially found using coin tapping, and then confirmed using c-scan. Crack growth did not go up dramatically since the patch is still transferring load over the cracked area as long as the patch remains bonded in the cracked area. The disbonding of the boron-epoxy patches under CA compression loading was already a serious indicator but was not yet conclusive since the loads that were used were not a direct representation of the actual loading conditions. Disbonding of the boron-epoxy patches under spectrum loading however disqualifies this repair for this particular application.

As can be seen from Figure 34 through Figure 36, the hybrid repairs are clearly performing the best, showing the smallest crack growth over two life times. None of the three hybrid repairs showed any signs of disbonding or delaminations after completion of the test, see appendix B.9. Also, no signs of patch cracking in the aluminum layer and no signs of patch tip failure in the skin were observed. Besides controlling the starter crack very well over two full life times, there was no crack initiation at any of the other rivet holes. Since the assumption is that there is no crack in the remaining substrate after making the grind-out, this is a good indication of the performance under realistic loading conditions.

All spectrum specimens showed crack growth that was meeting the symmetry requirements according to ASTM E647, or the adapted limits when taking the width of the grind-out as the determining width.

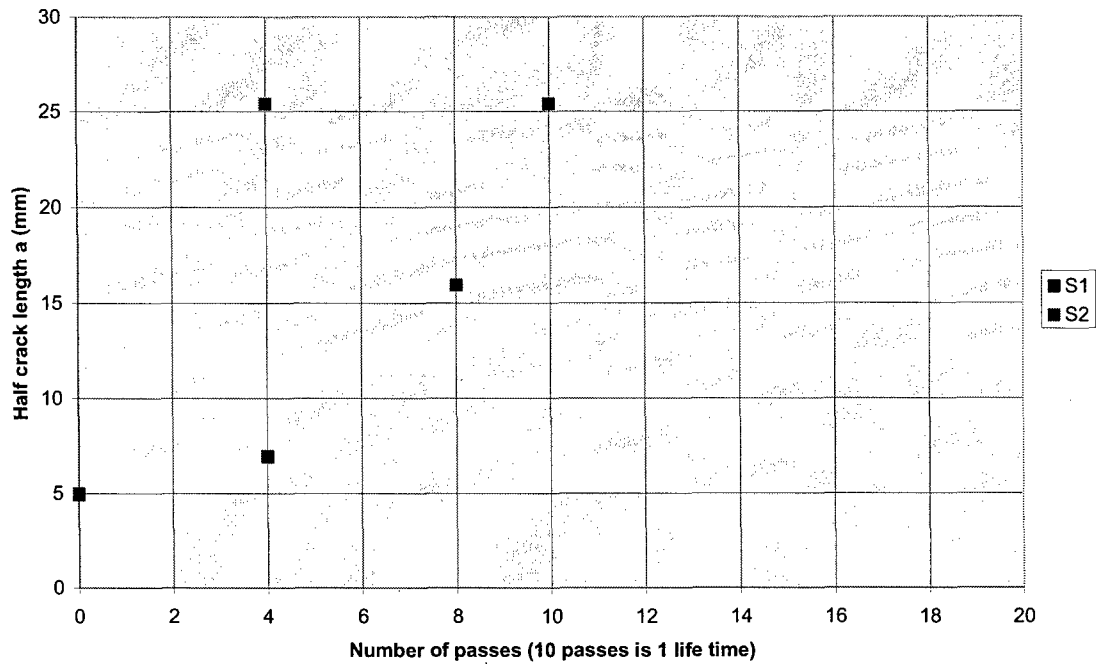


Figure 31: Specimens without repair, spectrum loading

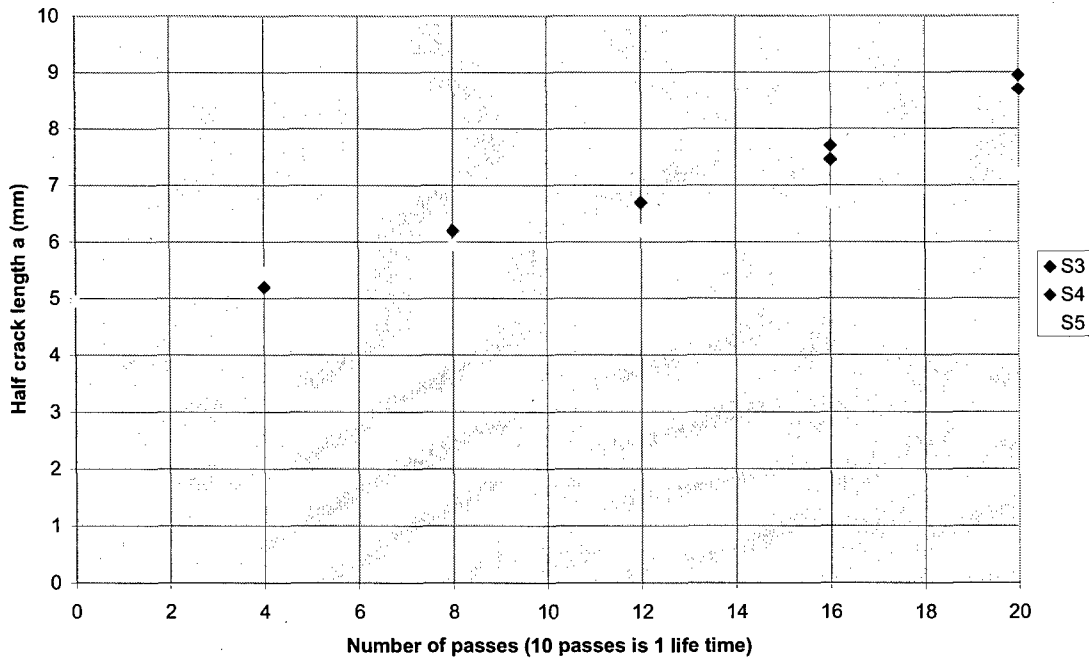


Figure 32: Specimens with aluminum repairs, spectrum loading

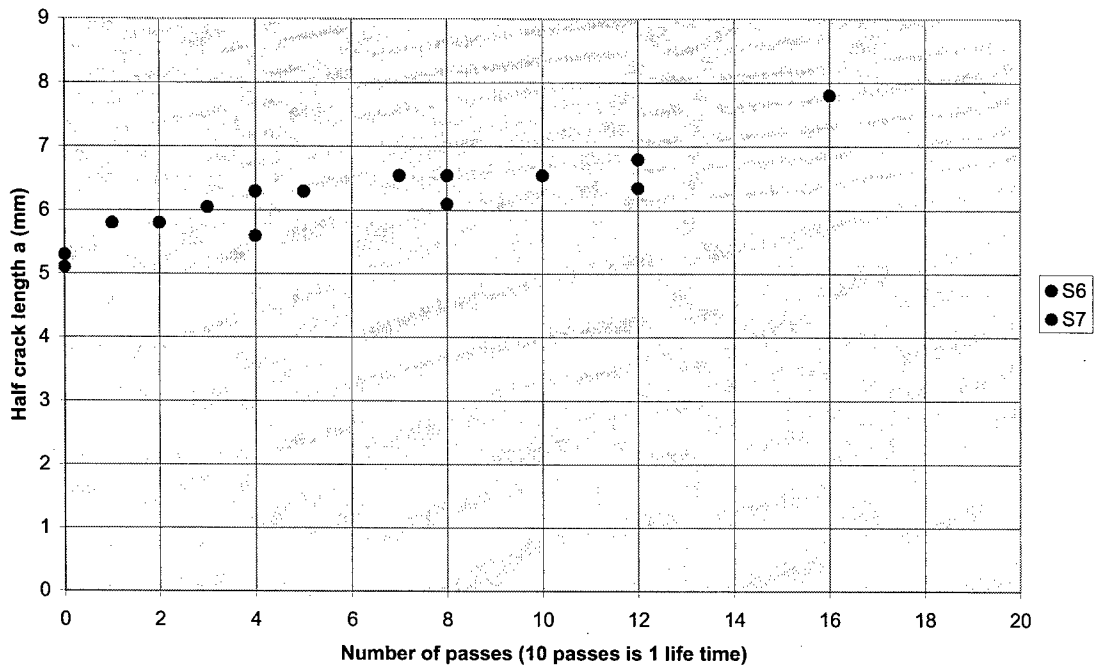


Figure 33: Specimens with boron-epoxy repairs, spectrum loading

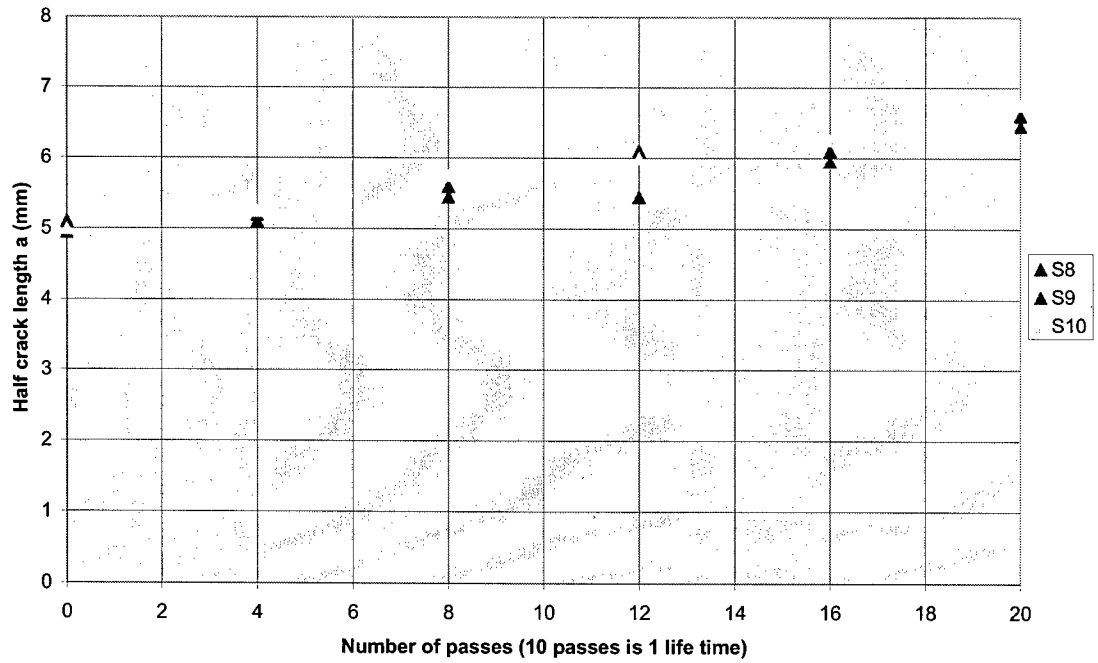


Figure 34: Specimens with hybrid repairs, spectrum loading

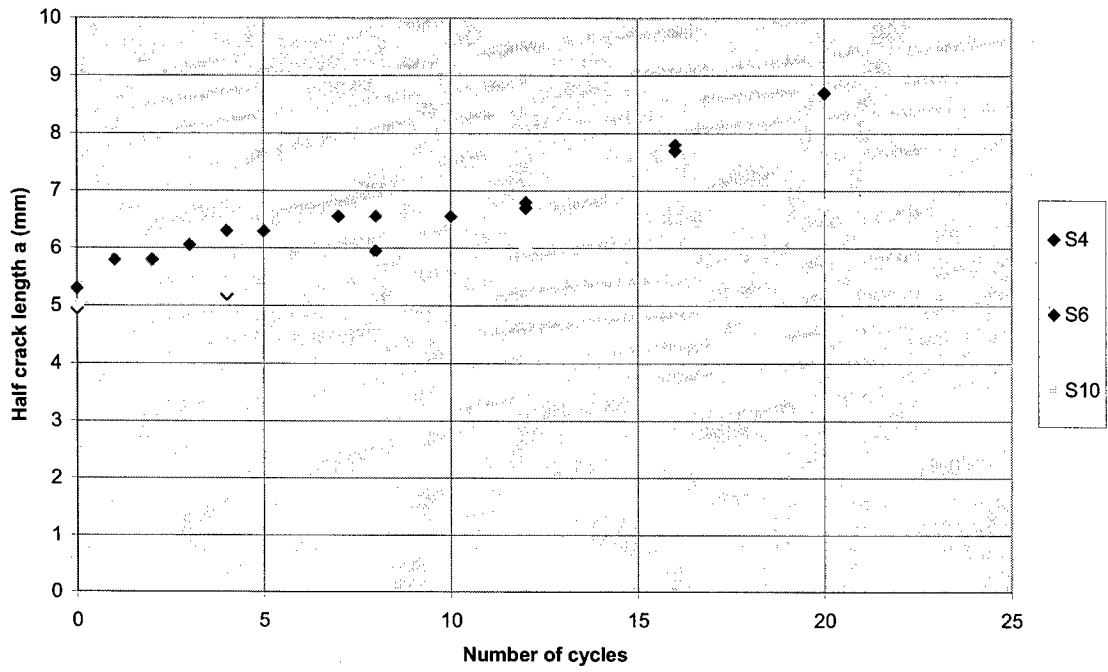


Figure 35: Spectrum specimens with three different repairs, spectrum loading

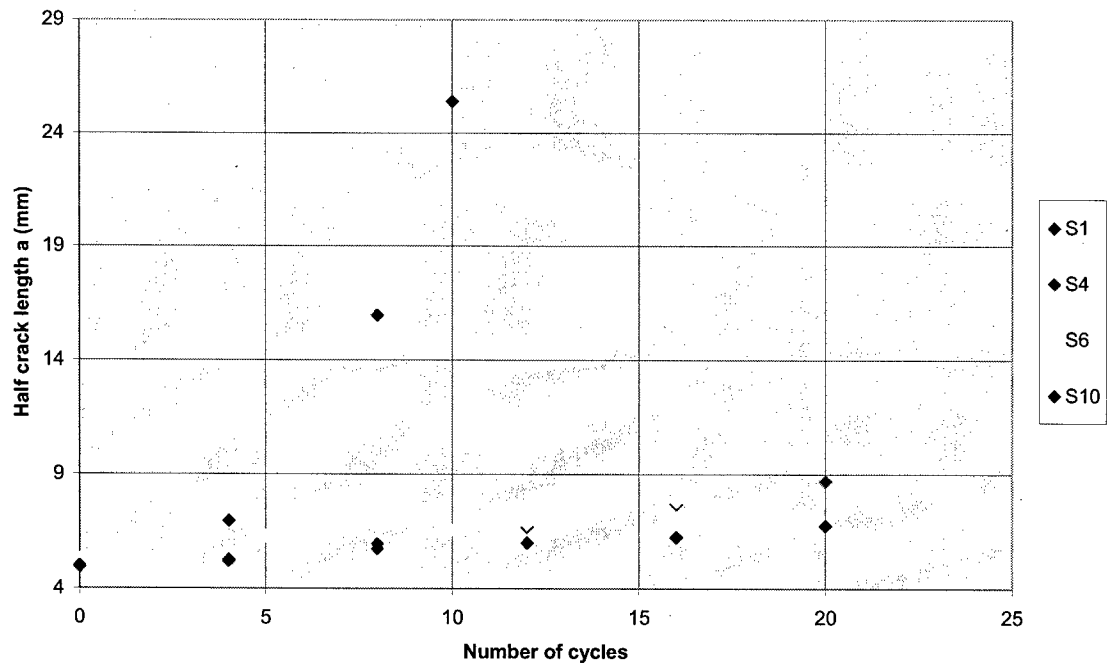


Figure 36: Spectrum specimens with and without repairs, spectrum loading

5. Conclusions

It was found that the application of a flush repair is a viable repair option in a compression dominated structure, for corrosion damage that is exceeding the current T.O. limits. Fatigue tests, both constant amplitude and spectrum loading, showed that from a durability standpoint the best options are either a hybrid repair or an aluminum repair.

Hybrid repairs are preferred based on the facts that they resulted in slowest crack growth rates, the patch being damage tolerant, and that they showed no signs of compression problems under realistic flight loading conditions

Since the hybrid repairs still use some boron-epoxy, there will still be thermal residual stresses after curing, as well as thermal stresses that occur while the aircraft is at operating temperature. In case these thermal stresses become a limiting factor, aluminum patches can be a good alternative, especially since it was found that the aluminum patches showed no patch cracking problems.

Furthermore, boron-epoxy should be avoided due to delamination problems under compressive fatigue loading, both constant amplitude and the more realistic spectrum loading.

The grind-outs were kept as small as possible during this project to prevent the removal of good material. This does however put pressure on some of the design guidelines for bonded repairs. Depending on the location, loading and operating temperature, the patches and therefore grind-outs could need re-sizing.

Finally, it was found that cracks can grow when loaded by a compression-compression fatigue cycle. This is caused by the thermal residual stresses that are left after bonding of the boron and hybrid patches.

6. Recommendations and Future Work

- Repair different grind-out depths (in progress). This becomes important when trying to repair a grind-out where a crack is present in the substrate. When grinding out less material, there is less depth available for the repair, while keeping the repair flush with the contour. It might not be possible to control this crack, since the repair will have a reduced stiffness ratio, especially since the high stiffness boron-epoxy has been ruled out as a repair material.
- Bonded repairs on top of actual exfoliation damage. Instead of removing the exfoliation, it might be possible to bond over the exfoliation, therefore avoiding making a grind-out. However, good NDI techniques will be needed in order to determine the depth of the exfoliation and/or possible crack. This is especially important for sizing the repair. If no good NDI is available, the repair must be sized based on full depth exfoliation or a through-crack, therefore making it necessary to transfer all load from the skin into the repair.
- DUL test. Besides proofing the durability of the repair under realistic fatigue loading, as was done during this program, structures with bonded repairs need to be able to withstand DUL.
- Fine-tuning of hybrid repair to optimize performance at operating temperature. Since the hybrid repair still has a considerable amount of boron-epoxy plies, there are residual thermal stresses present after bonding.
- Practical implementation of making the grind-outs on an aircraft

Acknowledgements

We would like to acknowledge the Aging Aircraft Support Squadron, Aeronautical Systems Center (ASC/AASS), Wright-Patterson AFB for funding this work.

References

- [1] Boeing Service Letter 707-SL-51-026, *Damage Identification and Removal During Structural Repairs*, 18 April 2003
- [2] T.O. 1C-135(K)A-3-4
- [3] *Composite Repairs to Metallic Structures Handbook (CRMS)*, AFRL/ML/TR-1998/4113
- [4] *Composite Materials and Adhesive Bonded Repairs*, RAAF Engineering Standard C5033
- [5] Byard, M., Danyluk, B., Dudley, B., Maggio, W., "Bonded Repair of Exfoliated Damage", EM460 report, 14 December 2004
- [6] Figure 3.2.3.1.6(a), page 3-95, Mil Handbook-5J, 31 January 2003
- [7] Griffin, K.E., Southwest Research Institute, "Bonded Composite Repair Efficiency For Highly Compression Loaded Thick Primary Structure, Final Report", SwRI Project No. 06-8476, Contract No. 1535EVF6S-05, Delivery Order 11049E-05, May 1998.
- [8] Chester, R., "Case History: F-111 Wing Pivot Fitting Reinforcement", in: Alan Baker, Francis Rose, Rhys Jones (Eds.), *Advances in the Bonded Composite Repair of Metallic Aircraft Structure*, Elsevier Science Ltd, Oxford, United Kingdom, 2002.
- [9] Guijt, C.B., Verhoeven, S., Greer, J.M., Van Galen, R.M., United States Air Force Academy, Center for Aircraft Structural Life Extension (CAStLE), DFEM/HQ USAFA, USA, "A New Approach to Manipulate Thermal Stresses in Bonded Repairs", Aging Aircraft 2002, San Francisco, California, 16-19 September 2002.
- [10] ASTM Standard E 647-00 "Standard Test Method for Measurement of Fatigue Crack Growth Rates"
- [11] Verhoeven, S., Guijt, C.B., Greer, Jr., J.M., Dinnebier, H., United States Air Force Academy, Center for Aircraft Structural Life Extension (CAStLE), DFEM/HQ USAFA, USA, Van Galen, R.M., Delft University of Technology, Faculty of Aerospace Engineering, Delft, The Netherlands, *Comparison of the Effectiveness of Glare and Boron-epoxy Patches in Repairs of Thin and Thick Structures, With and Without Secondary Bending*, Aging Aircraft 2001, Orlando, Florida, 10-13 September 2001.

Appendix A: Crack Growth Data

A.1 Unpatched Specimens, CA Loading

Cycles	Back left crack size a (mm) Eddy current	Back right crack size a (mm) Eddy current	Average a (mm) Eddy current	Corrected average a (mm)	Back left starter crack a (mm) Visual	Back right starter crack a (mm) Visual	Average starter crack a (mm) Visual
0	5	5.5	5.25	5	5.1	4.9	5
5000	25.4	18.5	21.95	21.7			

Table 9: a-N data for specimen CA1

Cycles	Back left crack size a (mm) Eddy current	Back right crack size a (mm) Eddy current	Average a (mm) Eddy current	Corrected average a (mm)	Back left starter crack a (mm) Visual	Back right starter crack a (mm) Visual	Average starter crack a (mm) Visual
0	6	5.5	5.75	5	5.1	4.9	5
1000	7	6.5	6.75	6			
2000	8	7	7.5	6.75			
3000	9	8	8.5	7.75			
4000	11	9.5	10.25	9.5			

Table 10: a-N data for specimen CA2

Cycles	Back left crack size a (mm) Eddy current	Back right crack size a (mm) Eddy current	Average a (mm) Eddy current	Corrected average a (mm)	Back left starter crack a (mm) Visual	Back right starter crack a (mm) Visual	Average starter crack a (mm) Visual
0	6	6.5	6.25	4.95	5	4.9	4.95
1000	7	6.5	6.75	5.45			
2000	7.5	7	7.25	5.95			
3000	7.5	7	7.25	5.95			
4000	8.5	8	8.25	6.95			
5000	9	8.5	8.75	7.45			
6000	9.5	9	9.25	7.95			
7000	11.5	10.5	11	9.7			

Table 11: a-N data for specimen CA3

Cycles	Back left crack size a (mm) Eddy current	Back right crack size a (mm) Eddy current	Average a (mm) Eddy current	Corrected average a (mm)	Back left starter crack a (mm) Visual	Back right starter crack a (mm) Visual	Average starter crack a (mm) Visual
0	6	6	6	5	4.9	5.1	5
1000	6	6	6	5			
2000	6.5	6.5	6.5	5.5			
3000	7.5	7	7.25	6.25			
4000	8	8	8	7			
5000	9.5	9	9.25	8.25			
6000	11	10.5	10.75	9.75			
7000	25.4	25.4	25.4	25.4			

Table 12: a-N data for specimen CA4

A.2 Specimens with Aluminum Repairs, CA Loading

Cycles	Back left crack size a (mm) Eddy current	Back right crack size a (mm) Eddy current	Average a (mm) Eddy current	Corrected average a (mm)	Back left starter crack a (mm) Visual	Back right starter crack a (mm) Visual	Average starter crack a (mm) Visual
0	5.5	5.5	5.5	5	5.1	4.9	5
10000	5.5	5.5	5.5	5			
20000	7	7	7	6.5			
30000	8	8.5	8.25	7.75			
40000	9.5	10	9.75	9.25			
50000	11	11.5	11.25	10.75			
60000	13.5	14	13.75	13.25			

Table 13: a-N data for specimen CA5

Cycles	Back left crack size a (mm) Eddy current	Back right crack size a (mm) Eddy current	Average a (mm) Eddy current	Corrected average a (mm)	Back left starter crack a (mm) Visual	Back right starter crack a (mm) Visual	Average starter crack a (mm) Visual
0	4.5	6	5.25	5.1	4.9	5.3	5.1
25000	6.5	7.5	7	6.85			
50000	9.5	10	9.75	9.6			
62500	11	11.5	11.25	11.1			
75000	14.5	14.5	14.5	14.35			

Table 14: a-N data for specimen CA6

Cycles	Back left crack size a (mm) Eddy current	Back right crack size a (mm) Eddy current	Average a (mm) Eddy current	Corrected average a (mm)	Back left starter crack a (mm) Visual	Back right starter crack a (mm) Visual	Average starter crack a (mm) Visual
0	5.5	5	5.25	5.05	5	5.1	5.05
10000	6	5.5	5.75	5.55			
20000	8	6	7	6.8			
30000	10	7.5	8.75	8.55			
40000	12	9	10.5	10.3			
50000	15	12.5	13.75	13.55			

Table 15: a-N data for specimen CA7

Cycles	Back left crack size a (mm) Eddy current	Back right crack size a (mm) Eddy current	Average a (mm) Eddy current	Corrected average a (mm)	Back left starter crack a (mm) Visual	Back right starter crack a (mm) Visual	Average starter crack a (mm) Visual
0	5.5	5	5.25	5.05	5.2	4.9	5.05
10000	6.5	6	6.25	6.05			
20000	8	7	7.5	7.3			
30000	9.5	8.5	9	8.8			
40000	11.5	10	10.75	10.55			
50000	13.5	12.5	13	12.8			

Table 16: a-N data for specimen CA8

A.3 Specimens with Boron-Epoxy Repairs, CA Loading

Cycles	Back left crack size a (mm) Eddy current	Back right crack size a (mm) Eddy current	Average a (mm) Eddy current	Corrected average a (mm)	Back left starter crack a (mm) Visual	Back right starter crack a (mm) Visual	Average starter crack a (mm) Visual
0	5.5	5.5	5.5	5	5.2	4.8	5
10000	6	5.5	5.75	5.25			
20000	6	5.5	5.75	5.25			
30000	6	5.5	5.75	5.25			
40000	7	5.5	6.25	5.75			
50000	8	6	7	6.5			
60000	9	7	8	7.5			
70000	10	7.5	8.75	8.25			
80000	11	8	9.5	9			
90000	12	8.5	10.25	9.75			
100000	13.5	9	11.25	10.75			

Table 17: a-N data for specimen CA9

Cycles	Back left crack size a (mm) Eddy current	Back right crack size a (mm) Eddy current	Average a (mm) Eddy current	Corrected average a (mm)	Back left starter crack a (mm) Visual	Back right starter crack a (mm) Visual	Average starter crack a (mm) Visual
0	6	5.5	5.75	5	5.1	4.9	5
10000	6	6	6	5.25			
20000	6.5	6	6.25	5.5			
30000	6.5	6.5	6.5	5.75			
40000	7	6.5	6.75	6			
50000	7.5	7	7.25	6.5			
60000	8	7	7.5	6.75			
70000	9.5	8	8.75	8			
80000	10	8.5	9.25	8.5			
90000	11	9.5	10.25	9.5			
100000	12	10	11	10.25			
110000	13	11	12	11.25			

Table 18: a-N data for specimen CA10

Cycles	Back left crack size a (mm) Eddy current	Back right crack size a (mm) Eddy current	Average a (mm) Eddy current	Corrected average a (mm)	Back left starter crack a (mm) Visual	Back right starter crack a (mm) Visual	Average starter crack a (mm) Visual
0	5.5	5.5	5.5	4.95	5	4.9	4.95
10000	5.5	5.5	5.5	4.95			
20000	5.5	6	5.75	5.2			
30000	6	6	6	5.45			
40000	6	6	6	5.45			
50000	6.5	6.5	6.5	5.95			
60000	7	7	7	6.45			
70000	7.5	7	7.25	6.7			
80000	8	7	7.5	6.95			
90000	9.5	8	8.75	8.2			
100000	10.5	9	9.75	9.2			
110000	11.5	10	10.75	10.2			
120000	13.5	10.5	12	11.45			

Table 19: a-N data for specimen CA11

Cycles	Back left crack size a (mm) Eddy current	Back right crack size a (mm) Eddy current	Average a (mm) Eddy current	Corrected average a (mm)	Back left starter crack a (mm) Visual	Back right starter crack a (mm) Visual	Average starter crack a (mm) Visual
0	5.5	5	5.25	5.1	5.3	4.9	5.1
10000	5.5	5.5	5.5	5.35			
20000	6	5.5	5.75	5.6			
30000	6.5	5.5	6	5.85			
40000	7	6	6.5	6.35			
50000	7.5	6.5	7	6.85			
60000	8.5	6.5	7.5	7.35			
70000	10	7.5	8.75	8.6			
80000	11.5	8.5	10	9.85			
90000	13.5	9.5	11.5	11.35			
100000	15.5	10.5	13	12.85			

Table 20: a-N data for specimen CA12

A.4 Specimens with Hybrid Repairs, CA Loading

Cycles	Back left crack size a (mm) Eddy current	Back right crack size a (mm) Eddy current	Average a (mm) Eddy current	Corrected average a (mm)	Back left starter crack a (mm) Visual	Back right starter crack a (mm) Visual	Average starter crack a (mm) Visual
0	5.5	5.5	5.5	5	4.8	5.2	5
10000	6	6	6	5.5			
20000	6.5	6	6.25	5.75			
30000	7	6.5	6.75	6.25			
40000	7.5	7	7.25	6.75			
50000	8	7.5	7.75	7.25			
60000	8.5	8	8.25	7.75			
70000	9	8.5	8.75	8.25			
80000	9.5	9	9.25	8.75			
90000	10.5	9.5	10	9.5			
100000	11.5	10.5	11	10.5			
110000	12	11.5	11.75	11.25			

Table 21: a-N data for specimen CA13

Cycles	Back left crack size a (mm) Eddy current	Back right crack size a (mm) Eddy current	Average a (mm) Eddy current	Corrected average a (mm)	Back left starter crack a (mm) Visual	Back right starter crack a (mm) Visual	Average starter crack a (mm) Visual
0	5.5	5.5	5.5	5	5.1	4.9	5.0
10000	6	6	6	5.5			
20000	6.5	6	6.25	5.75			
30000	7	6.5	6.75	6.25			
40000	7.5	6.5	7	6.5			
50000	8.5	7	7.75	7.25			
60000	10	7.5	8.75	8.25			
70000	11	8	9.5	9			
80000	12	8.5	10.25	9.75			
90000	13.5	9.5	11.5	11.5			

Table 22: a-N data for specimen CA14

Cycles	Back left crack size a (mm) Eddy current	Back right crack size a (mm) Eddy current	Average a (mm) Eddy current	Corrected average a (mm)	Back left starter crack a (mm) Visual	Back right starter crack a (mm) Visual	Average starter crack a (mm) Visual
0	5.5	5.5	5.5	5.05	5	5.1	5.05
10000	5.5	5.5	5.5	5.05			
20000	6	6	6	5.55			
30000	6.5	6	6.25	5.8			
40000	6.5	6.5	6.5	6.05			
50000	7	7	7	6.55			
60000	8	7.5	7.75	7.3			
70000	8.5	8	8.25	7.8			
80000	9	8.5	8.75	8.3			
90000	10	9.5	9.75	9.3			
100000	11	10.5	10.75	10.3			
110000	12	11.5	11.75	11.3			
120000	13.5	13.5	13.5	13.5			

Table 23: a-N data for specimen CA15

Cycles	Back left crack size a (mm) Eddy current	Back right crack size a (mm) Eddy current	Average a (mm) Eddy current	Corrected average a (mm)	Back left starter crack a (mm) Visual	Back right starter crack a (mm) Visual	Average starter crack a (mm) Visual
0	5.5	5.5	5.5	5	5	5	5
10000	6	6	6	5.5			
20000	6.5	7	6.75	6.25			
30000	7	8	7.5	7			
40000	7.5	9.5	8.5	8			
50000	8.5	10	9.25	8.75			
60000	9	11	10	9.5			
70000	9.5	12	10.75	10.25			
80000	11	14	12.5	12			

Table 24: a-N data for specimen CA16

A.5 Unpatched Specimens, Spectrum Loading

Spectrum passes	Back left crack size a (mm) Eddy current	Back right crack size a (mm) Eddy current	Average a (mm) Eddy current	Corrected average a (mm)	Back left starter crack a (mm) Visual	Back right starter crack a (mm) Visual	Average starter crack a (mm) Visual
0	6.5	5.5	6	4.95	5	4.9	4.95
4	8.5	7.5	8	6.95			
8	18	16	17	15.95			
10	25.4	25.4	25.4	25.4			

Table 25: a-N data for specimen S1

Spectrum passes	Back left crack size a (mm) Eddy current	Back right crack size a (mm) Eddy current	Average a (mm) Eddy current	Corrected average a (mm)	Back left starter crack a (mm) Visual	Back right starter crack a (mm) Visual	Average starter crack a (mm) Visual
0	5.5	5	5.25	5	5.3	4.7	5
4	25.4	25.4	25.4	25.4			

Table 26: a-N data for specimen S2

A.6 Specimens with Aluminum Repairs, Spectrum Loading

Spectrum passes	Back left crack size a (mm) Eddy current	Back right crack size a (mm) Eddy current	Average a (mm) Eddy current	Corrected average a (mm)	Back left starter crack a (mm) Visual	Back right starter crack a (mm) Visual	Average starter crack a (mm) Visual
0	5.5	5.5	5.5	4.95	4.9	5	4.95
4	6	6	6	5.45			
8	7	6.5	6.75	6.2			
12	7.5	7	7.25	6.7			
16	8	8	8	7.45			
20	9.5	9.5	9.5	8.95			

Table 27: a-N data for specimen S3

Spectrum passes	Back left crack size a (mm) Eddy current	Back right crack size a (mm) Eddy current	Average a (mm) Eddy current	Corrected average a (mm)	Back left starter crack a (mm) Visual	Back right starter crack a (mm) Visual	Average starter crack a (mm) Visual
0	5.5	5.5	5.5	4.95	4.9	5	4.95
4	5.5	6	5.75	5.2			
8	6.5	6.5	6.5	5.95			
12	7	7.5	7.25	6.7			
16	8	8.5	8.25	7.7			
20	9	9.5	9.25	8.7			

Table 28: a-N data for specimen S4

Spectrum passes	Back left crack size a (mm) Eddy current	Back right crack size a (mm) Eddy current	Average a (mm) Eddy current	Corrected average a (mm)	Back left starter crack a (mm) Visual	Back right starter crack a (mm) Visual	Average starter crack a (mm) Visual
0	6	5	5.5	4.95	5	4.9	4.95
4	6.5	5.5	6	5.45			
8	7	6	6.5	5.95			
12	7	6.5	6.75	6.2			
16	7.5	7	7.25	6.7			
20	8	7.5	7.75	7.2			

Table 29: a-N data for specimen S5

A.7 Specimens with Boron-Epoxy Repairs, Spectrum Loading

Spectrum passes	Back left crack size a (mm) Eddy current	Back right crack size a (mm) Eddy current	Average a (mm) Eddy current	Corrected average a (mm)	Back left starter crack a (mm) Visual	Back right starter crack a (mm) Visual	Average starter crack a (mm) Visual
0	5.5	5.5	5.5	5.3	5.5	5.1	5.3
1	6	6	6	5.8			
2	6	6	6	5.8			
3	6	6.5	6.25	6.05			
4	6.5	6.5	6.5	6.3			
5	6.5	6.5	6.5	6.3			
7	7	6.5	6.75	6.55			
8	7	6.5	6.75	6.55			
10	7	6.5	6.75	6.55			
12	7	7	7	6.8			
16	8	8	8	7.8			

Table 30: a-N data for specimen S6

Spectrum passes	Back left crack size a (mm) Eddy current	Back right crack size a (mm) Eddy current	Average a (mm) Eddy current	Corrected average a (mm)	Back left starter crack a (mm) Visual	Back right starter crack a (mm) Visual	Average starter crack a (mm) Visual
0	5	6	5.5	5.1	4.6	5.6	5.1
4	5.5	6.5	6	5.6			
8	6	7	6.5	6.1			
12	6	7.5	6.75	6.35			

Table 31: a-N data for specimen S7

A.8 Specimens with Hybrid Repairs, Spectrum Loading

Spectrum passes	Back left crack size a (mm) Eddy current	Back right crack size a (mm) Eddy current	Average a (mm) Eddy current	Corrected average a (mm)	Back left starter crack a (mm) Visual	Back right starter crack a (mm) Visual	Average starter crack a (mm) Visual
0	5.5	5.5	5.5	5.1	5.1	5.1	5.1
4	5.5	5.5	5.5	5.1			
8	6	6	6	5.6			
12	6.5	6.5	6.5	6.1			
16	6.5	6.5	6.5	6.1			
20	7	7	7	6.6			

Table 32: a-N data for specimen S8

Spectrum passes	Back left crack size a (mm) Eddy current	Back right crack size a (mm) Eddy current	Average a (mm) Eddy current	Corrected average a (mm)	Back left starter crack a (mm) Visual	Back right starter crack a (mm) Visual	Average starter crack a (mm) Visual
0	5.5	5.5	5.5	4.95	4.8	5.1	4.95
4	6	5.5	5.75	5.2			
8	6	6	6	5.45			
12	6	6	6	5.45			
16	6.5	6.5	6.5	5.95			
20	7	7	7	6.45			

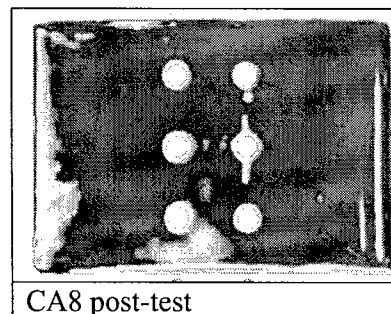
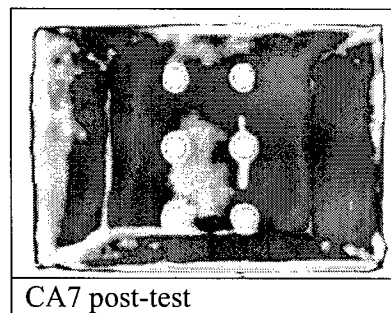
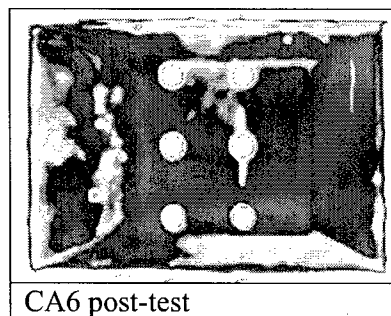
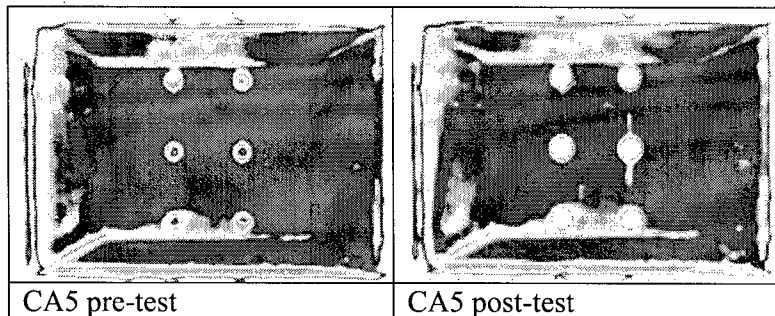
Table 33: a-N data for specimen S9

Spectrum passes	Back left crack size a (mm) Eddy current	Back right crack size a (mm) Eddy current	Average a (mm) Eddy current	Corrected average a (mm)	Back left starter crack a (mm) Visual	Back right starter crack a (mm) Visual	Average starter crack a (mm) Visual
0	5.5	5.5	5.5	5	4.7	5.3	5
4	5.5	6	5.75	5.25			
8	6	6.5	6.25	5.75			
12	6.5	6.5	6.5	6			
16	6.5	7	6.75	6.25			
20	7	7.5	7.25	6.75			

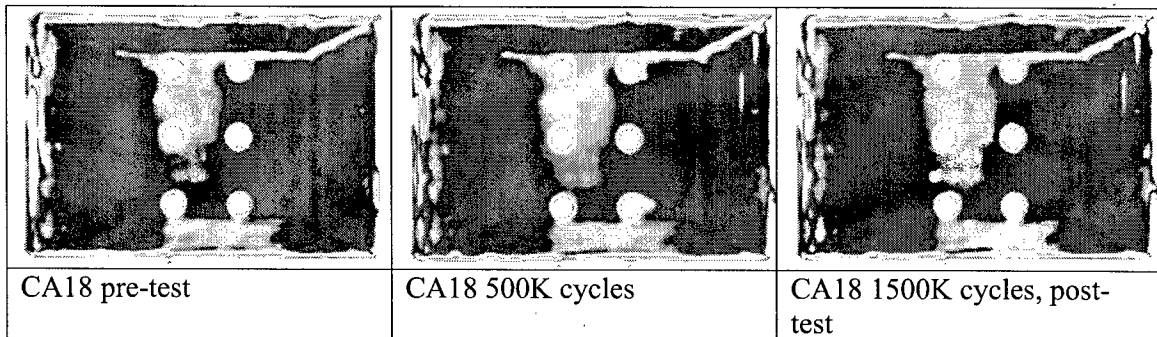
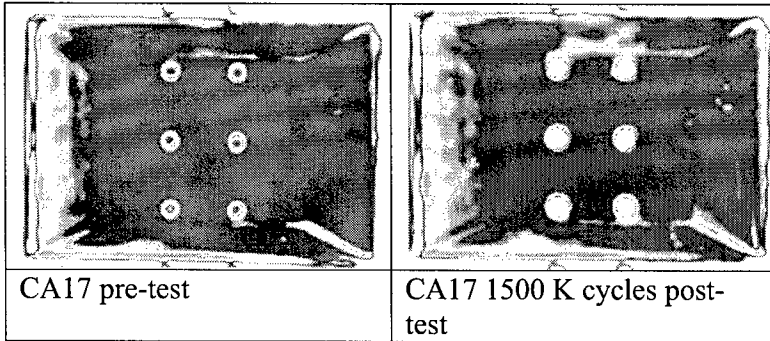
Table 34: a-N data for specimen S10

Appendix B: C-Scan Images

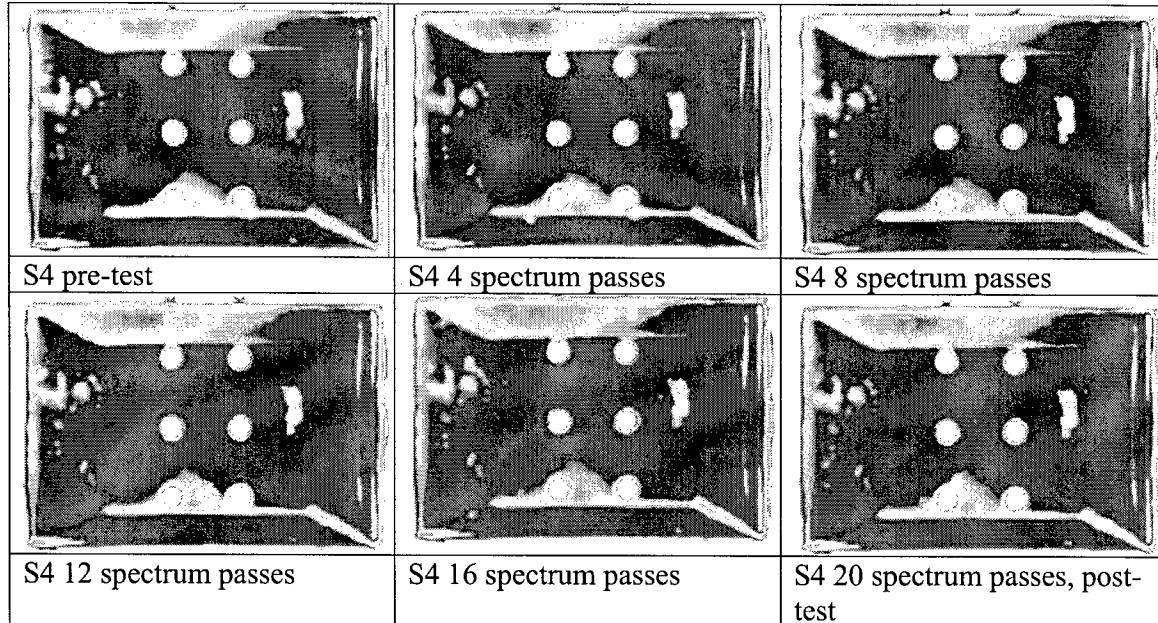
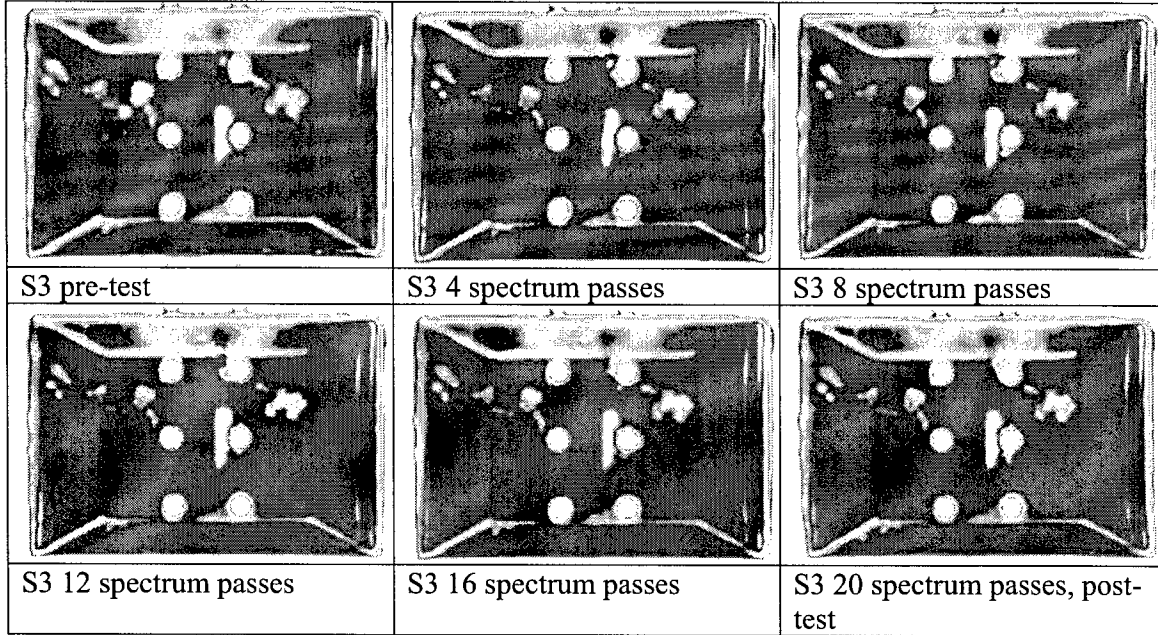
B.1 Specimens with Aluminum Repairs, CA Tension Loading

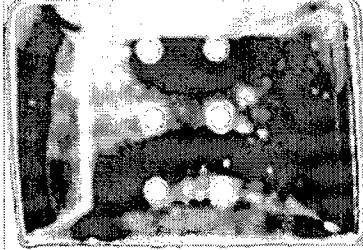
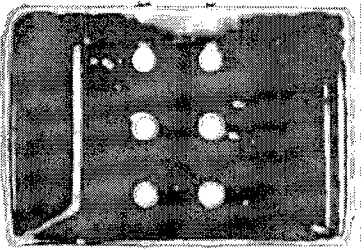
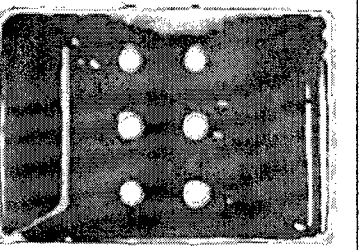
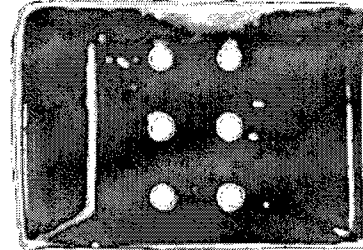
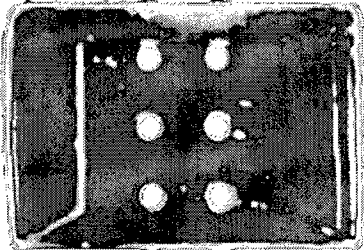
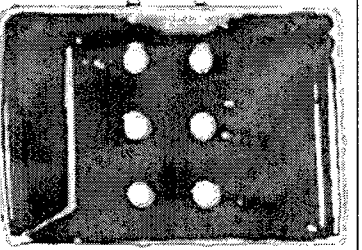


B.2 Specimens with Aluminum Repairs, CA Compression Loading



B.3 Specimens with Aluminum Repairs, Spectrum Loading



		
S5 pre-test	S5 4 spectrum passes	S5 8 spectrum passes
		
S5 12 spectrum passes	S5 16 spectrum passes	S5 20 spectrum passes, post-test

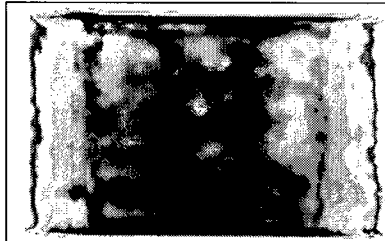
B.4 Specimens with Boron-Epoxy Repairs, CA Tension Loading



CA9 post-test



CA10 post-test

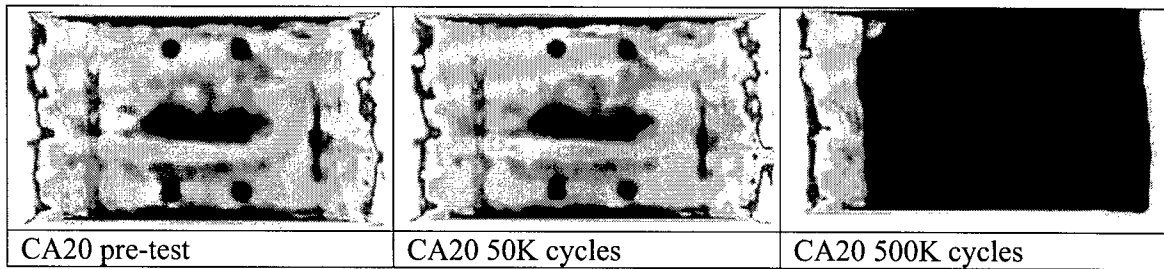
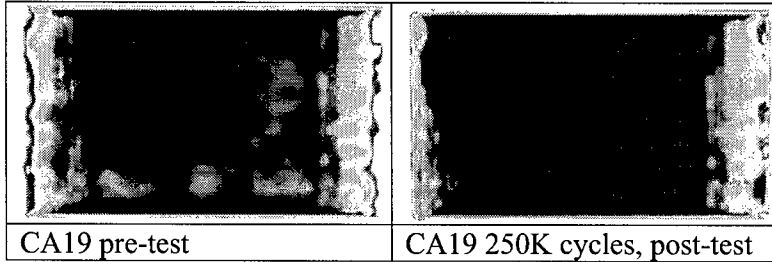


CA11 post-test



CA12 post-test

B.5 Specimens with Boron-Epoxy Repairs, CA Compression Loading



B.6 Specimens with Boron-Epoxy Repairs, Spectrum Loading



S6 16 spectrum passes, post-test



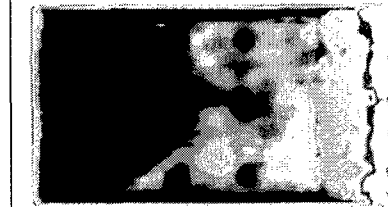
S7 pre-test



S7 4 spectrum passes

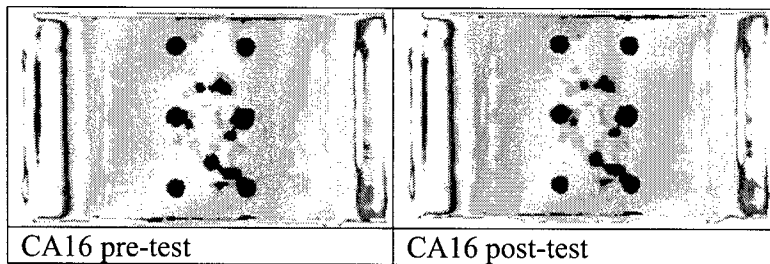
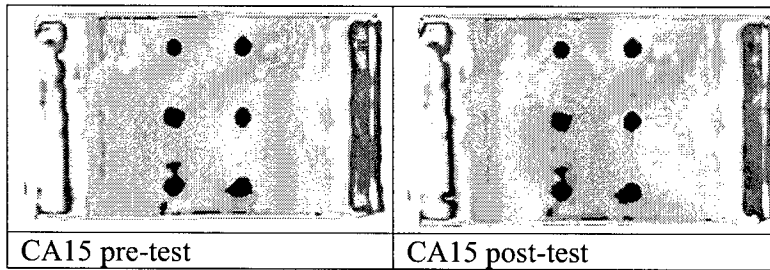
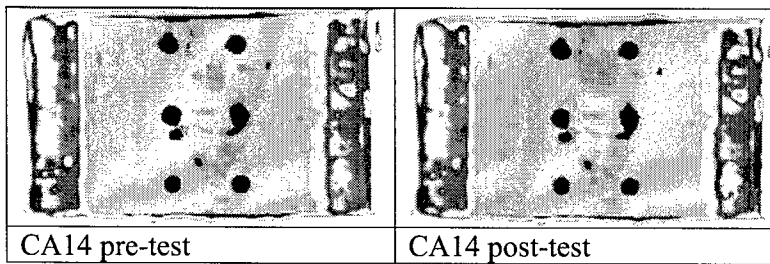
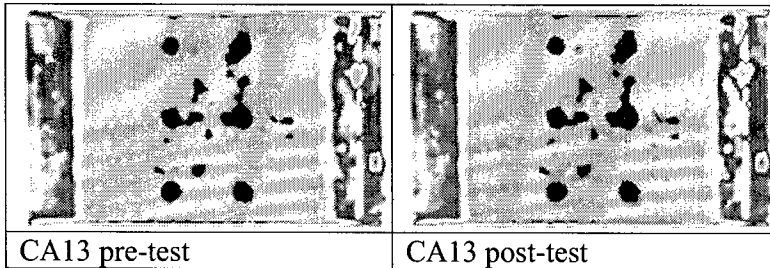


S7 8 spectrum passes

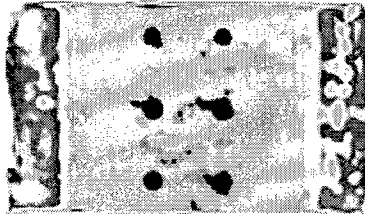
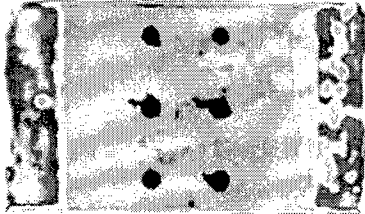
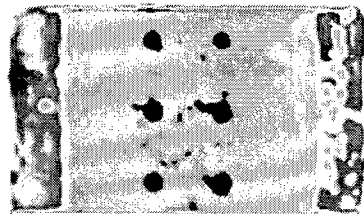
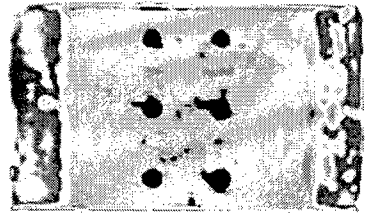
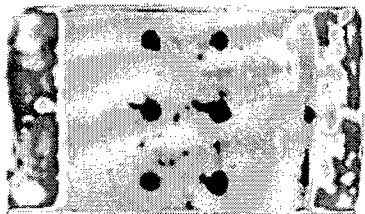


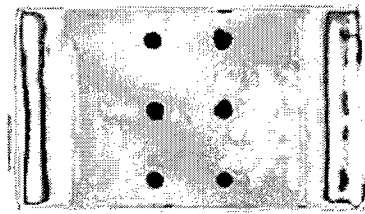
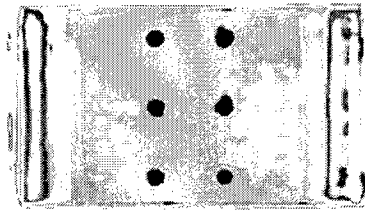
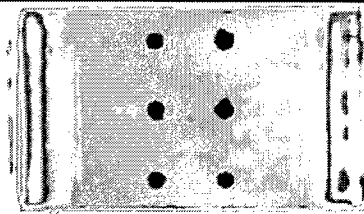
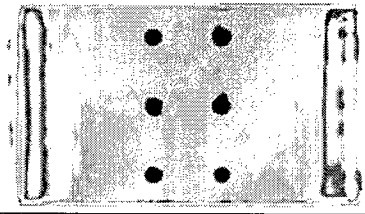
S7 12 spectrum passes

B.7 Specimens with Hybrid Repairs, CA Tension Loading

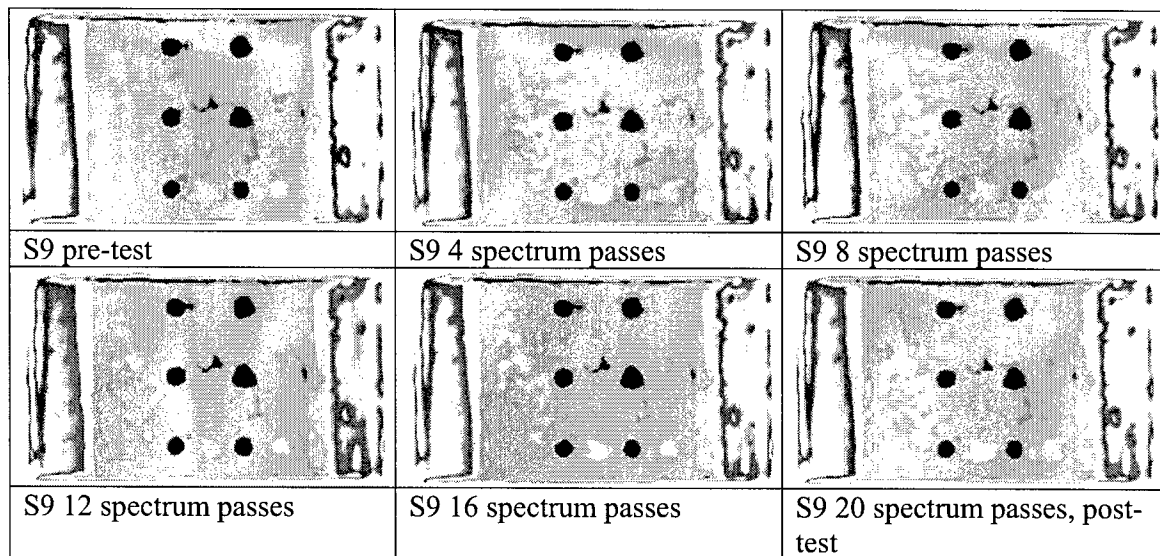
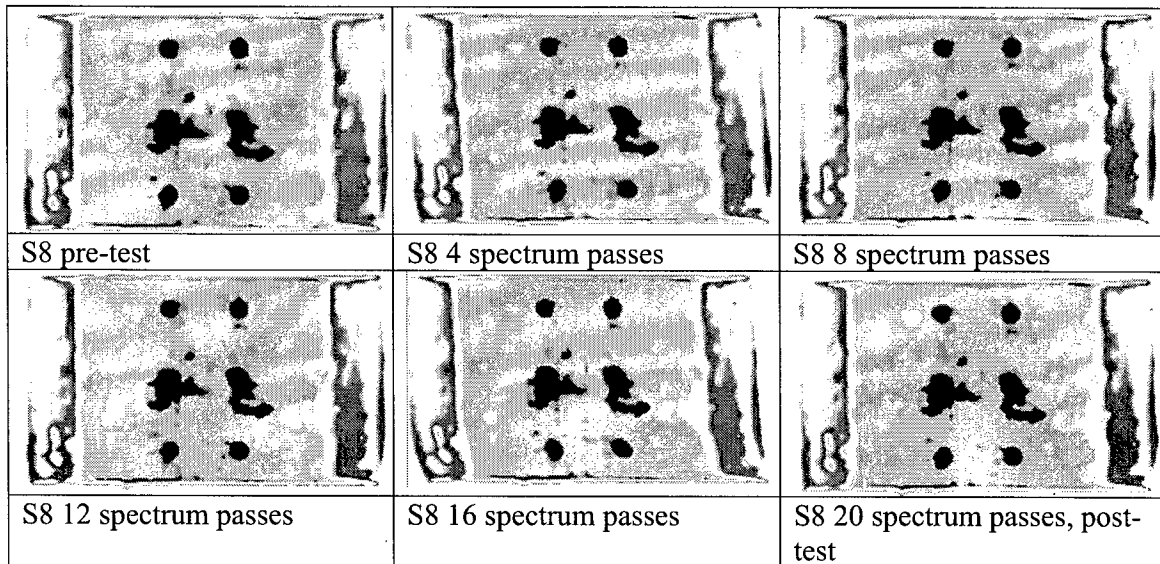


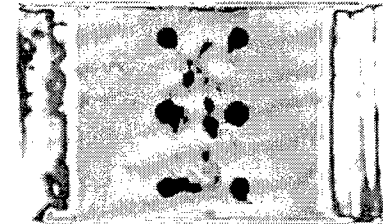
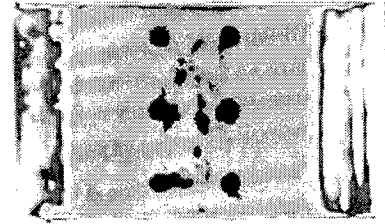
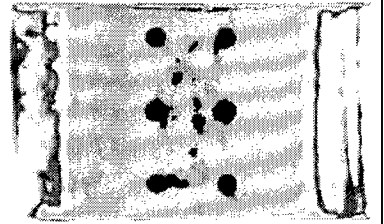
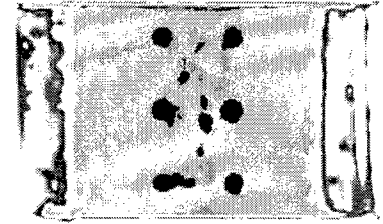
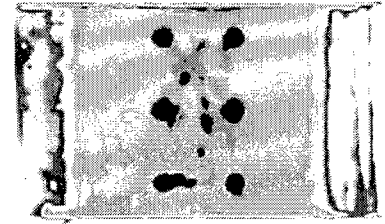
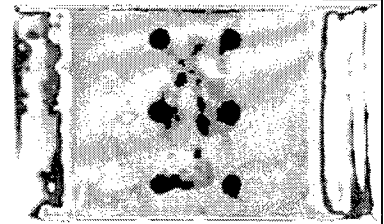
B.8 Specimens with Hybrid Repairs, CA Compression Loading

		
CA21 pre-test	CA21 100K cycles	CA21 500K cycles
		
CA21 1000K cycles	CA21 1500K cycles, post test	

		
CA 22 pre-test	CA22 500K cycles	CA22 1000K cycles
		
CA22 1500K cycles		

B.9 Specimens with Hybrid Repairs, Spectrum Loading



		
S10 pre-test	S10 4 spectrum passes	S10 8 spectrum passes
		
S10 12 spectrum passes	S10 16 spectrum passes	S10 20 spectrum passes, post-test